UNDERSTANDING THE ROLE OF SUTURES IN CRANIAL MECHANO-MORPHOGENESIS.

by

PRINCE ODAME

(Under the Direction of GUIGEN ZHANG)

ABSTRACT

The general purpose of this study was to perform finite element analysis (FEA) on 2D and 3D models of the cranium to determine the stress distribution and the stress components at the bone/suture interface. Two-dimensional and 3D models of the cranium were built using ALGOR (Pittsburgh, PA) and PROENGINEER WILDFIRE (CAD software). Linear and nonlinear analyses were performed on the models, mimicking various conditions that exist in craniosynostosis. The distribution of the stresses at the bone/suture interface was obtained by plotting the stress values along the length of the suture. To help elucidate the internal stress states at the bone/suture interface, 2D and 3D Mohr's circles were constructed at peak and valley locations along the sagittal suture. The 2D models revealed that at the peak locations where there are high shear stresses and biaxial tension and compression, bone resorption may occur and at the valley location where there are small shear and tensile stresses bone growth may occur. The stress distribution along the bone/suture interface in the 3D model of the cranium indicates that there is high tensile stress in the upper layer of the suture, and high compressive stress in the inner layer. This nature of stress distribution explains why the pattern of interdigitation on the outer surface of the sutures is different from that on the inside, and offers an explanation as to why suture fusion starts from the inside surface of the cranium.

INDEX WORDS: Craniosynostosis, Mechano-morphogenesis, FEA, Mohr's circles, Cranial suture, Plagiocephaly, ALGOR.

UNDERSTANDING THE ROLE OF SUTURES IN CRANIAL MECHANO-

MORPHOGENESIS

by

PRINCE ODAME

B.S, Kwame Nkrumah University of Science and Technology, Ghana, 2001

A Thesis Submitted to the Graduate Faculty of The University of Georgia in Partial Fulfillment of the Requirements for the Degree

MASTER OF SCIENCE

ATHENS, GEORGIA

2004

UNDERSTANDING THE ROLE OF SUTURES IN CRANIAL MECHANO-

MORPHOGENESIS

by

PRINCE ODAME

Major Professor: Guigen Zhang

Committee: Jack Yu
William S. Kisaalita
Chi Thai
James Borke

Electronic Version Approved:

Maureen Grasso
Dean of the Graduate School
The University of Georgia
December 2004

To my family for their love and support

ACKNOWLEDGEMENTS

Special thanks to my major professor Dr. Guigen Zhang, for his open-minded guidance, constructive criticisms, direction, patience and encouragement during the entire course of my Masters study. I also thank Drs, Jack Yu, James Borke, Chi Thai and William S. Kisaalita for serving on my advisory committee and providing me with guidance and new ideas.

I am very grateful to Paul Bowles and the technical team at ALGOR for their technical support, and to Mike Yoder for providing me with skulls to guide me in the modeling process.
I also want to thank my friends and colleagues in the Agricultural and Bioengineering Department for their companionship and for sharing their research experience. I also thank all the people in the Department for their assistance, which was available whenever needed.

Last but not the least, I thank my parents, brother and sisters for their constant encouragement and support throughout my life; to them I dedicate my further studies.

TABLE OF CONTENTS

CHAPTER 1

INTRODUCTION

Sutures are fibrous structures that join the neighboring cranial bone plates, and they are major sites of cranial bone growth. To allow normal cranial development, sutures must remain in an unossified state. Premature ossification of sutures (or craniosynostosis) hinders further bone formation at their growth fronts and may lead to abnormal brain growth, altered head shape, retardation, or learning disability. To be able to prevent these adverse consequences, there is a need to know the conditions that will keep a suture patent or cause it to ossify prematurely.

Over the years, significant research efforts have been focused on the development of cranial sutures and bones. On one hand, there is a vast body of knowledge regarding the growth factors and transcription factors that regulate suture patency and cranial bone development (Opperman, 2002), while on the other hand, there is some trace evidence of the mechanical influence on cranial base cartilage and sutural growth. Given the mechanical conditions (or environment) being the proximate cause and the transcriptional events the effect, our limited knowledge about the mechanical environment has led to an information disjunction. It has been known for years that mechanical stresses modulate biological tissue development. But, will all stresses have the same effect, or will knowing that certain mechanical loading causes some stimulatory events provide us sufficient information to link this disjunction? The answers are both negative.

It is thus hypothesized that the actual internal mechanical stress states at the bone growth fronts, not the externally applied loads, govern the development of cranial bones and sutures.

The overall goal of this research is to validate this hypothesis using 2D and 3D finite element analysis (FEA). FEA is a powerful reverse engineering tool that will enable us to create 2D and 3D models of the cranium and at the same time calculate the stress states at any location in the models. This capability will help determine the stress components and their magnitudes that exist at the bone/suture interface.

A literature review describing craniosynostosis and its various forms and also explaining the biomechanics of bone is outlined in chapter two. The hypothesis and objectives of the research is laid out in chapter three. Chapter four talks about the modeling considerations of the 2D model and the results and discussions from the various studies done with the model. In chapter five the results and discussion of a study to incorporate the nonlinearity of bone into the modeling is presented. Chapter six focuses on the 3D modeling discussing the results and outlining the possible links to the mechano-morphogenesis of the cranial suture. Conclusions from all the studies done in this research are presented in chapter seven and the possible future research ideas are outlined in chapter eight.

CHAPTER 2

LITERATURE REVIEW

Cranial Development and Plagiocephaly

Sutures are fibrous structures that join the neighboring cranial bone plates, and represent major sites of cranial bone growth (Opperman, 2002). They intersect in certain areas of the skull forming fontanelles. There are about five sutures in the cranium namely sagittal, coronal, metopic, lambdoid and squamosal (see Figure 1 and Figure 2). The bones of the cranium are mainly frontal, parietal, temporal, and occipital, as shown in Figure 1 and Figure 2, and they are well developed by the fifth month of gestation (Khan et al., 2003).

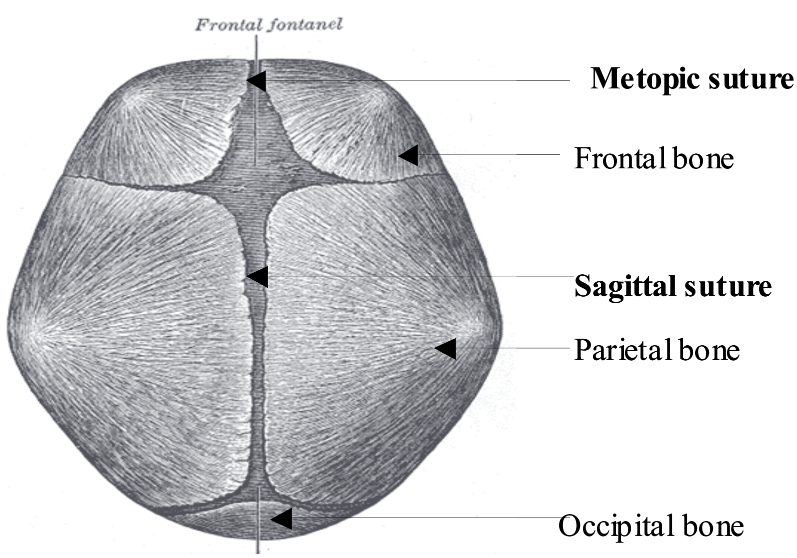

Figure 1 Top View of skull (Grays Anatomy, 1918) showing the cranial bones and sutures.

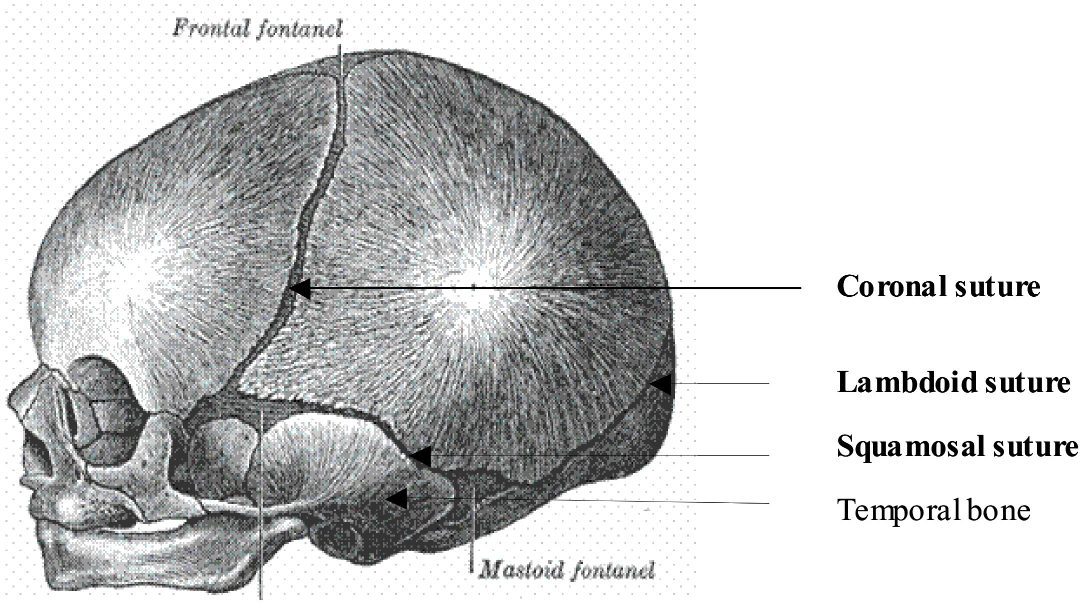

Figure 2 Side views of skull (Grays Anatomy, 1918) showing cranial bones and sutures.

The cranium lodges and protects the brain. The cranial bones have a composite structure and they exhibit nonlinear mechanical properties. The composite structure consists of cancellus or trabecular bone sandwiched by compact or cortical bone. Both the cortical and cancellus layers are hybrids of hydroxyapatite minerals oriented in collagen polymer, with the cancellus being spongier (Porter, 2003; Currey J, 1984). The sagittal suture separates the two parietal bones, the coronal suture separates the two frontal bones from the parietal bones, the metopic suture separates the frontal bones, the lambdoid suture separates the occipital bone from the two parietal bones and the squamosal suture separates the temporal bones from the parietal bones. These sutures remain patent to allow the brain to fully develop before they finally ossify. Periods of ossification differ from suture to suture. Some ossify as early as nine months and others ossify as late as the ages of 30 to 40 years (Aviv et al., 2001).

Plagiocephaly refers to cranial asymmetry and occurs at a rate of 5% - 12% in live births in this country (Alderman et al., 1988; Argenta et al., 1996; Baxter et al., 2000; Cohen, 2001; Ellenbogen et al., 2000; Kelly et al., 1999; Perlyn et al., 2001; Miller et al., 2000; Aliberti et al., 2002). Synostotic plagiocephaly (craniosynostosis) refers to the closure (or premature ossification) of one or more of the cranial sutures (Aviv et al., 2001). Craniosynostosis can be classified into primary and secondary. Also classification into non-syndromic and syndromic craniosynostosis is commonly used in clinical practice with the syndromic ones due to syndromes and the non-syndromic ones not due to syndromes. Craniosynostosis is said to be simple when only one suture fuses prematurely, and complex or compound when there is premature fusion of multiple sutures.

Primary craniosynostosis results from a primary defect of ossification. This could be simple non-syndromic, complex syndromic or complex non-syndromic. There are about five forms of simple non-syndromic craniosynostosis depending on which suture fuses (see Figure 3). They are scaphocephaly, trigonocephaly, anterior plagiocephaly, brachycephaly and posterior plagiocephaly. Early fusion of the sagittal suture is known as scaphocephaly; early fusion of one coronal suture is known as anterior plagiocephaly; early bilateral coronal suture fusion is known as brachycephaly; early fusion of one lambdoid suture is known as posterior plagiocephaly; early fusion of the metopic suture is known as trigonocephaly. Craniosynostosis is seen in a variety of syndromes, which all together are referred to as syndromic craniosynostosis. The most common syndromes encountered in clinical practice are Crouzon, Apert, Saethre- Chotzen, and Pfeiffer. These syndromes are often characterized by bilateral coronal synostosis of varying severity, often combined with some degree of sagittal synostosis (Sheth et al., 2001; Wolf et al., 2000).

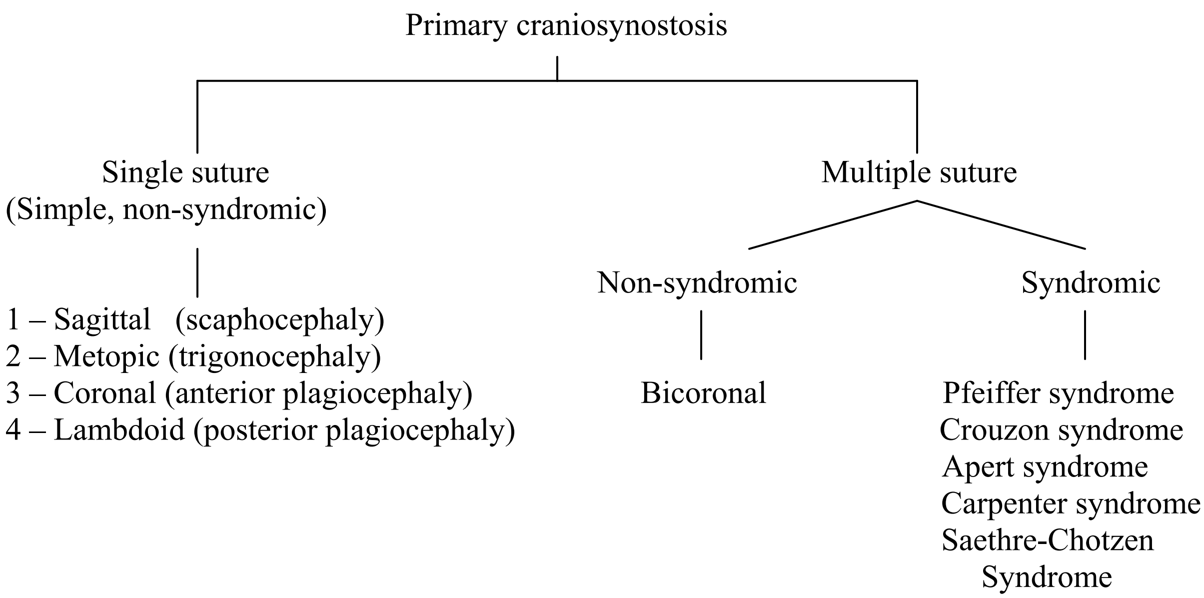

Figure 3 Tree diagram showing the classification of Primary craniosynostosis into single and multiple sutures.

The syndromic craniosynostosis is believed to result from genetic mutations responsible for FGF2 and FGF3 receptors (Sheth et al., 2001; Wolf et al., 2000). The most widely accepted theory for the possible cause of primary craniosynostosis is the primary defect in the mesenchymal layer ossification in the cranial bones.

Secondary craniosynostosis results typically from systemic disorders and early fusion of sutures due to failure of brain growth. Failure of brain growth results in a form of craniosynostosis called microcephaly. Some of these disorders include

1. Endocrine- hyperthyroidism, hypophosphatemia, vitamin D deficiency, renal osteodystrophy, hypercalcemia, and rickets;
2. Hematologic disorders that cause bone marrow hyperplasia (e.g., sickle cell disease, thalassemia);

3. Inadequate brain growth including microcephaly and its causes and shunted hydrocephalus.

It is also believed that intrauterine space constraints and multiple pregnancy may play a role in the premature fusion of sutures in the fetal skull. Sometimes as a result of positional molding, plagiocephaly may occur. In this case children have a flattened posterior part of the head on one or both sides without having premature fusion of the lambdoid sutures. This and other forms of plagiocephaly do not require surgery, as the others usually do. Therefore differentiating this from the other forms of plagiocephaly is extremely important (Sheth et al., 2001; Aviv et al., 2001).

Apart from the obvious clinical deformity affecting the face and head, children can have airway problems, especially children with the syndromic form of craniosynostosis. Because of the hypoplastic maxilla, these children have difficulty breathing through their nose and end up breathing through their mouth. At night these children can have sleep apnea. This affects not only their growth pattern, but also their behavior and speech. Children with raised intracranial pressure (ICP) often exhibit of chronic headaches, declining school performance, and gradual visual failure. The loss of the sutural growth fronts also leads to abnormal brain development, altered head shape, retardation and aberrations, or learning disability. As children grow, abnormal facial appearance has a negative effect on their social integration, with a corresponding effect on personality development (Sgouros et al., 2003; Aviv et al., 2001).

About 1% of the infants with plagiocephaly have the synostotic form (or craniosynostosis). Incidence of craniosynostosis is 0.04% - 0.1 %. Of affected individuals, 2% - 8% have primary craniosynostosis. The remaining cases are secondary craniosynostosis, which frequently is accompanied by microcephaly. Premature fusion of the sagittal suture is the most common craniosynostosis constituting more than half (50%-58%) of all cases (Sheth et al., 2001; Aviv et al., 2001). It occurs frequently in premature infants. The frequencies of the other types of craniosynostosis are as follows: coronal 20% -29%, metopic 4% -1 0%, and lambdoid 2% - 4% (Sheth et al., 2001; Williams J.K et al., 1999).

There is therefore a need to understand the mechanism of craniosynostosis to help control or prevent its occurrence and to better treat it in order to prevent its adverse consequences.

Mechanics of Bone and Cranial Mechano-morphogenesis

Mechanical adaptation of bone is the process whereby living bone adapts its mass and structure to prevailing mechanical usage to obtain a higher efficiency of load bearing. The form of adult bone is regulated by two main factors. The first is the predetermined genetic template that explains individual differences in the general size of bones between individuals. The second is the fact that bone as a tissue is able to react to changes in the level of mechanical loading and, as suggested by Wolff, will respond to both the magnitude and pattern of loading. Thus in the absence of mechanical loading, the form of a skeletal element will revert to the basic genetically determined bone mass (Henderson, J.H et al., 2002). Evidence supporting the fact that bones remodel according to the mechanical environments is as follows:

Chalmers and Ray performed a classic experiment in which the cartilaginous anlage of the femur in developing mice was transplanted into the spleen, a site devoid of mechanical loading (Chalmers, J et al., 1962). After development, the bone was compared with that which developed under normal physiological loading. Although the bone developed as a recognizable femur, it lacked the refinements associated with the normal functional bone (see Figure 4). The major features induced by function (aid in locomotion) were organization of the internal trabecular structure, the width of the medullary cavity and thickness of the cortical wall, the waisting of the femoral neck, and the curvature of the femoral diaphysis. Thus any reduction in the functional loading of a bone induces modeling changes that reduce the mass and revert the form to that of the basic genetic template.

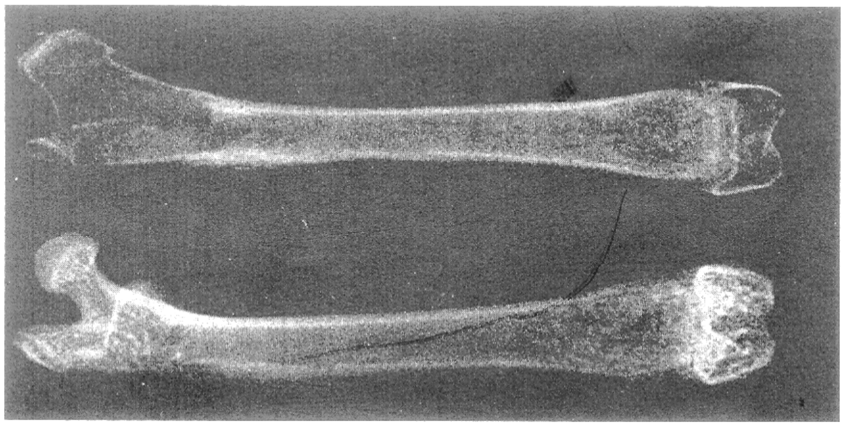

Figure 4 (Bottom) Murine femur showing normal morphology developed within a normal functional environment. (Top) Femur developed from the cartilage anlage after transplantation to the spleen, devoid of mechanical loading and showing the form associated with the genetic template alone (Cowin S.C, 2001).

Fell also conducted studies on cultured chick limb primordia and observed that some of the prominences on specific bones developed in culture and some did not (Fell, H.B , 1956). This was interpreted as some bony features required functional loading for development whereas others were part of the genetic template (Cowin, S.C, 2001).

For an imposed tension or pressure to act as an inductive signal there must be a mechanism of mechanotransduction through which the cell translates the mechanical signal into a particular biological response. Thus changes in functional loading induce a cellular response to model the bone to an optimal mass to withstand the imposed load as suggested by Wolff's concept which states that bone mass is related to the magnitude of the prevailing load. The schematic diagram in Figure 5 shows how mechanical loading induces cellular responses and eventually bone formation. Mechanotransduction includes two important steps: (1) mechanosensing – the step where the physical signal derived from matrix strain is sensed by the cells and translated into a biological signal; and (2) intercellular signaling – the step where biological signals are used to activate osteoblasts and osteoclasts.

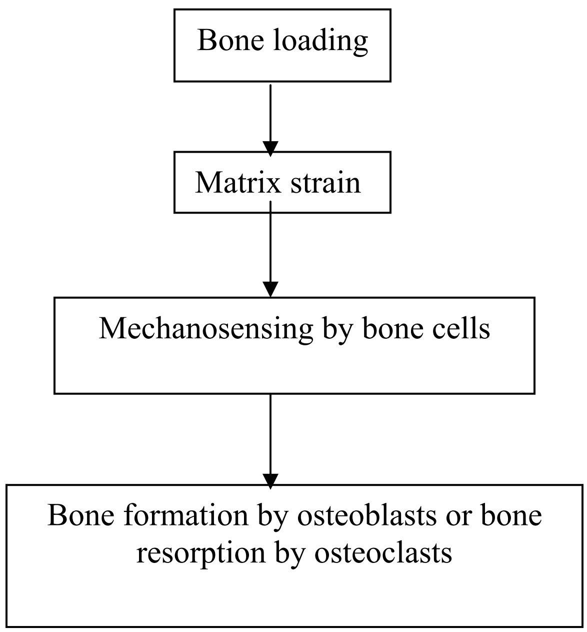

Figure 5 Schematic diagram showing the induction of cellular responses by mechanical loading.

Sutures induce bone formation by responding to mechanical stresses exerted on them. The induced biomechanical stresses cause cellular biochemical responses that result in either osteoblast or osteoclast. The growth of the cranial bones occur in a direction perpendicular to the sutures and when the suture fuses, growth becomes parallel to the sutures. (Sheth et al., 2001; Khan et al., 2003; Aviv et al., 2001).

The mechanical stresses experienced in the cranium may be partly due to growth generated stresses. The terms growth generated strains and growth generated stresses are used to refer to the local deformations and corresponding internal force intensities that are created by differential growth in developing tissues. It is believed that when cells in a tissue divide, mature and hypertrophy, the individually produced pressures combine over a region of tissue to form a significant source of cell-generated pressure (Henderson et al., 2002). The growth of the brain also generates a pressure called intracranial pressure (ICP), which is transmitted to the cranium via the *dura mata*. The likelihood of raised ICP is dependent on the number of fused sutures, i.e., the greater the number of fused sutures the greater the ICP (Aviv et al., 2001). The sutures sense this pressure as a tensile force, which results as the bone plates tend to move apart to accommodate the developing brain. The sutures sensing this stress initiate certain chemical responses to result in growth of bone in a direction perpendicular to the sutures. When one or more of the sutures have synostosed, expansion of the cranium to accommodate the developing brain is impeded, thus creating an increase in the intracranial pressure. Stresses in the brain are also due to heartbeat and respiration. This is supported by the observation that one can feel the upward and downward movements of the fontanels in newborn babies as they respire. Also, masticatory activities introduce stresses in the cranium.

It is now established through diverse research that cranial morphogenesis is a result of the mechanical stresses sensed by the sutures. The formation and evolution of suture interdigitation is controlled by its mechanical environment. The increased interdigitation seen in the coronal and posterior frontal sutures between the two antlers in a deer skull when compared to sutures in regions more distal from the antlers supports this view (see Figure 6). This increased interdigitation is certainly related to the excessive forces and stresses that are generated from activities of the deer.

These known stresses are mostly indirect or external stresses which is not the same nature (tensile, compressive or shear) and magnitude sensed by the sutures. This is so because of the nature of the cranial bones (anisotropic) and the orientation of the suture to the applied stress and the pattern of the suture. Also, as in the osseous structure of a femur, the trabecular bone architecture follows the exact pattern of its stress trajectories i.e. orientations of the principal stresses. This evidence offers a powerful testimony that the ossified trabecular architecture is not only the biological record of the past biomechanical events, but more precisely the record of the internal stress states in the femur (see Figure 7).

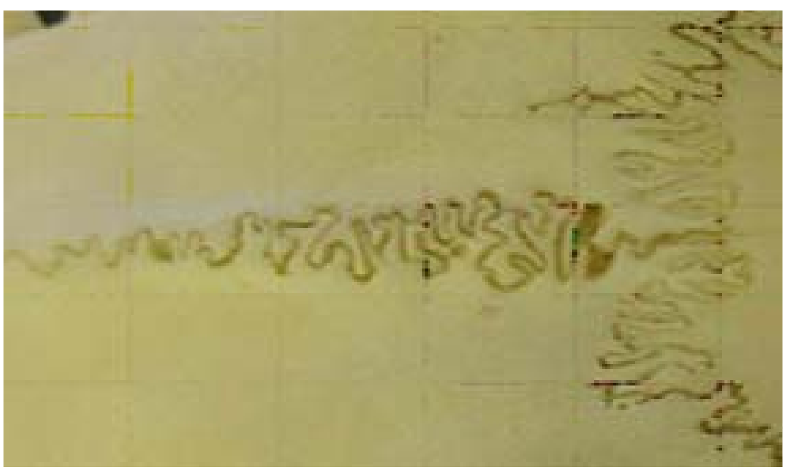

Figure 6 The coronal and posterior frontal sutures in a deer skull. Suture interdigitation increases between the two antlers.

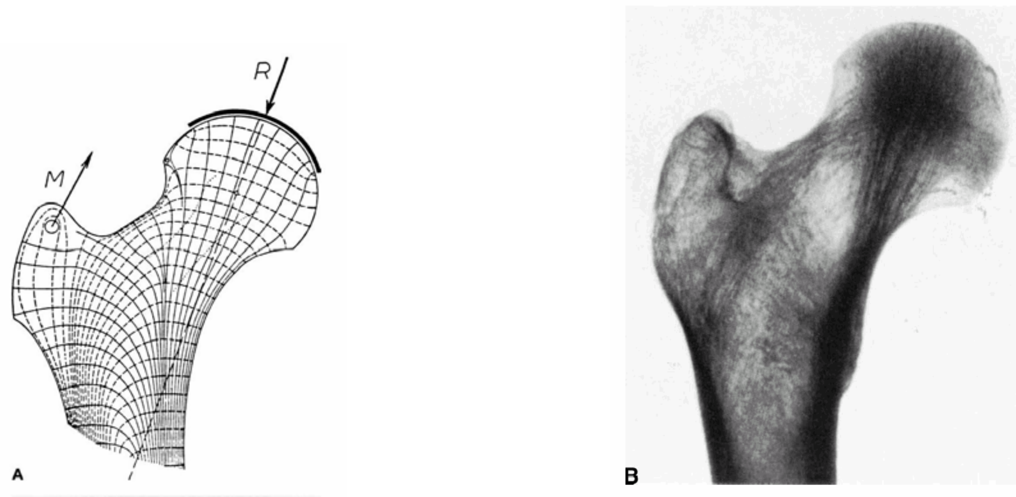

Figure 7 Stress trajectories (A) and cancellus bone architecture (B) in a femur (Turner, 1998).

It is believed that different kinds and magnitudes of stresses (tensile, compressive and shear) induce different cellular responses that result in either bone formation or resorption along the bone/suture interface. It has been known for years that mechanical loading modulates the structural remodeling process of the cranial bones, however what is not clear is how the processes unfold and the exact component and level of the stresses. Thus, there is a compelling need to elucidate the biomechanics that govern the biological modulating processes (Klein et al., 1987; Zhang et al., 1996; Gilbert et al., 1999; Frost, 1963; Richtsmeier et al., 2002, Vu et al., 2001; Turk et al., 1996; Enlow, 1975, 2002). To elucidate the biomechanics that govern the biological modulating processes, efforts should be devoted to understand how the external loading is converted to the internal stress states and subsequently how these internal stress states activate or inhibit certain biochemical effects. It is therefore important to study the nature and magnitude of the stresses at the bone/suture interface to better understand the conditions that keep the sutures patent or the conditions that causes craniosynostosis.

CHAPTER 3

HYPOTHESIS AND OBJECTIVES

It has been hypothesized that the actual internal mechanical stress states at the bone fronts govern the development of cranial bones and sutures. This hypothesis will be validated using 2D and 3D FEA studies to investigate the internal stress state along a wavy bone/suture interface.

Cranial bones are three-dimensional structures that exist in a 3D environment. The 3D environment presents us with a loading condition at the bone/suture interface that is more complicated than the loading condition in the 2D environment. In 3D there are three planes on which the load can act compared to the one plane of load action in 2D. This kind of loading condition results in six stress states, which combines to give three principal normal and shear stresses. The questions then are, which of the stress states and magnitudes govern the morphology of the suture, are the stress states and their corresponding magnitudes uniform along the depth of the bone/suture interface?

To help determine the components of the stresses and their magnitudes Mohr's circles were constructed at the bone/suture interface. Mohr's circle contains the information of the entire stress states at a given location. A 3D model will also present the ability to construct 3D Mohr's circles that will represent the loading conditions (the magnitude of tensile, compressive and shear stresses) on all three planes.

The overall goal is to elucidate the stress states at the bone/suture interface that would help shed light on the morphology of the cranial sutures. To achieve this goal, the following specific aims are identified.

Specific Aims

Specific aim 1**:** *To perform a two dimensional finite element analysis to determine the stress distribution that exists along the bone/suture interface.*

To help establish a linkage between the internal stress states and the mechano-mophogenesis of the suture, a 2D model will be built and linear analysis performed. It is believed that between the bone and sutures there is an interphase that has neither the properties of bone nor sutures. To model the thin layer between bone and suture, which is neither bone nor suture, an interphase will be added between the bone and suture. Also the fusion of sutures will be simulated by gradually reducing the width of the sutures.

Specific aim 2**:** *To determine the stress states at the bone/suture interface considering the nonlinear nature of the bone.*

The cranial bone plates are nonlinear materials so their stress-strain curve follows a nonlinear pattern. To incorporate this behavior of bone into our analysis and thus mimicking the *in vivo* condition, it is important that the nonlinear behavior of bones be considered.

Specific aim 3**:***To perform a three-dimensional finite element analysis to determine the stress distribution that exists along the bone/suture interface in a cranial model.*

To correlate the 3D stress states at the bone fronts and suture morphology, a 3D investigation of a bone/suture structure under static loading will be performed. The cranium will be modeled with sinusoidal suture patterns embedded in it. To gain insight into multiple birth pregnancy in which the heads of the fetuses are in contact and thus inducing compressive forces on the area of contact, a compressive load will be added to the medial lateral side of the 3D model. Also an infant cranium with properties of infant bone and suture will be analyzed under static loading. As bone ages its properties change and so the way it deforms when a load is applied to it also changes. It is believed that the infant cranium will react differently to loading as a result of its different material properties. Also the various synostotic forms will be mimicked. It is believed that when synostosis occurs in one suture the sutures nearest to it take over the remodeling of the skull. To verify this, the various forms of synostosis will be simulated and the results compared to the model in which all the sutures are patent.

CHAPTER 4

TWO DIMENSIONAL FINITE ELEMENT STUDY OF THE STRESS DISTRIBUTION AT THE BONE/SUTURE INTERFACE

Modeling Considerations

Sutures *in vivo* have a uniform width. However modeling of a suture with uniform width proved difficult. This was because sketching a wavy curve and simply copying and shifting it to form the suture, resulted in a nonuniform width suture. Therefore a uniform width suture was modeled based on mathematical theorems and derivations as outlined below. The equation $y = AzSin\omega z$ was used to generate a sinusoidal curve A as shown in Figure 8 (left).

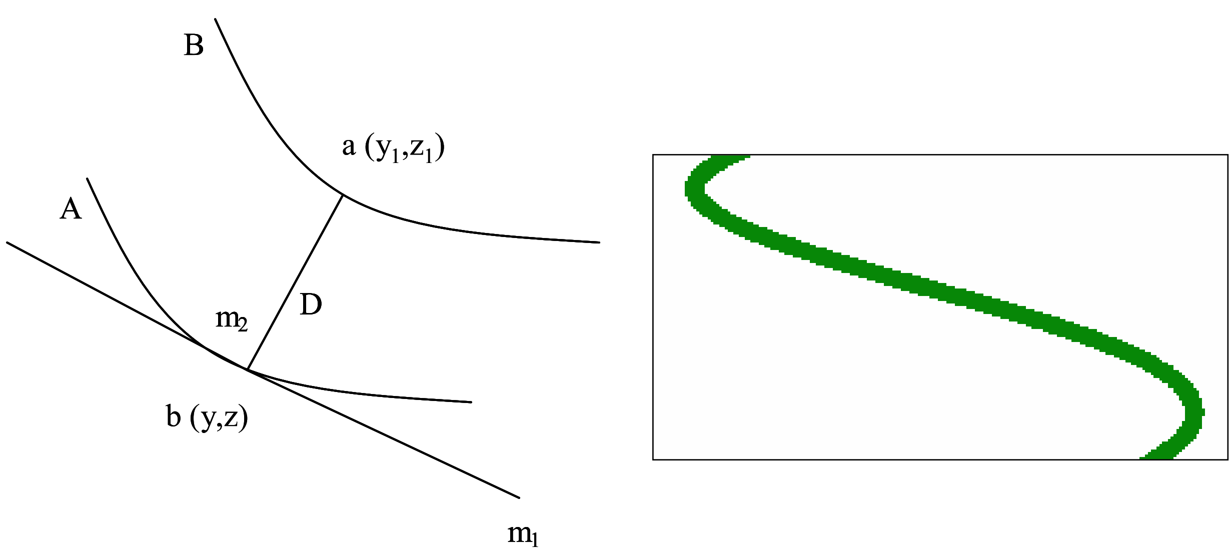

Figure 8 Left: A sketch showing how a suture with a constant width was derived. Right: uniform width suture.

B is another curve which is to be created at a constant distance D from curve *A*. Points *a* and *b* are end points of the straight line *D* with slope m_2 which is perpendicular to the tangent of curve *A*, m_1. The tangent of *A* is the differential of the equation of *A*. Mathematically $m_1 \times m_2 = -1$ and the distance between points *a* and *b,* D is given by the equation $D = \left((z - z_1)^2 + (y - y_1)^2\right)^{1/2}$. Using the slopes of the curve A and line D, the relationship between two perpendicular lines and the equation for the distance between the points *a* and *b*, the equations for z_1 and y_1 were determined. This yielded an equation for z_1 as $z_1 = (A\omega z \cos\omega z + A\sin\omega z)(y - y_1) + z$ and that for y_1 as $y_1 = y + D/\left((A\omega z\cos\omega z)^2 + A^2(\sin\omega z)^2 + 2A^2\omega z\cos\omega z \times \sin\omega z + 1\right)^{1/2}$. Therefore for each point *a*(*z,y*) on the sinusoidal curve *A*, a corresponding point *b*(z_1,y_1) at a distance of 0.15mm from *A* was derived. Data points for the two curves were generated and imported into the FEA software, ALGOR. This yielded a suture with uniform width (Figure 8, right). The FEA model consisted of a bone/suture/bone structure with a dimension of 10mm×4.75mm, with a strip of suture of 0.15mm width embedded in between the bones as shown in Figure 8. The bone and suture were meshed using 2-D quadrilateral elements with a mesh size of 0.05mm for the bone and 0.009mm for the suture. This resulted in a very fine mesh, which produced normal stress continuity at the interface. One end of the model was fixed and the other end loaded with a load of 3.3KPa. This value was derived by making use of the formulae for stress in the walls of spherical pressure vessels given by $\sigma = \Pr/2t$, where P is pressure, r is radius and t is thickness. For the material properties the bone was assigned a Young modulus (E) of 8420MPa and Poisson ratio (ν) of 0.28, and the suture, 50MPa and 0.4 respectively. These values were derived based on laminated composite theory along with mechanical properties and volume fractions of the cortical and cancellus bone.

To incorporate an interphase between the bone and suture, bone elements adjacent to the suture elements were selected and new material properties assigned to them (Figure 9). The material properties used were the summation of half the material properties of both bone and sutures. Thus a Young modulus of 4235MPa and a Poisson ratio of 0.35 were assigned to the interphase.

To investigate the effect of fusion of sutures, sutures of width of 0.01mm, 0.02mm, 0.03mm, 0.04mm and 0.05mm were used (see Figure 10). This was to simulate the reduction in width of the suture as the suture cells adjacent to the bone turn into bone.

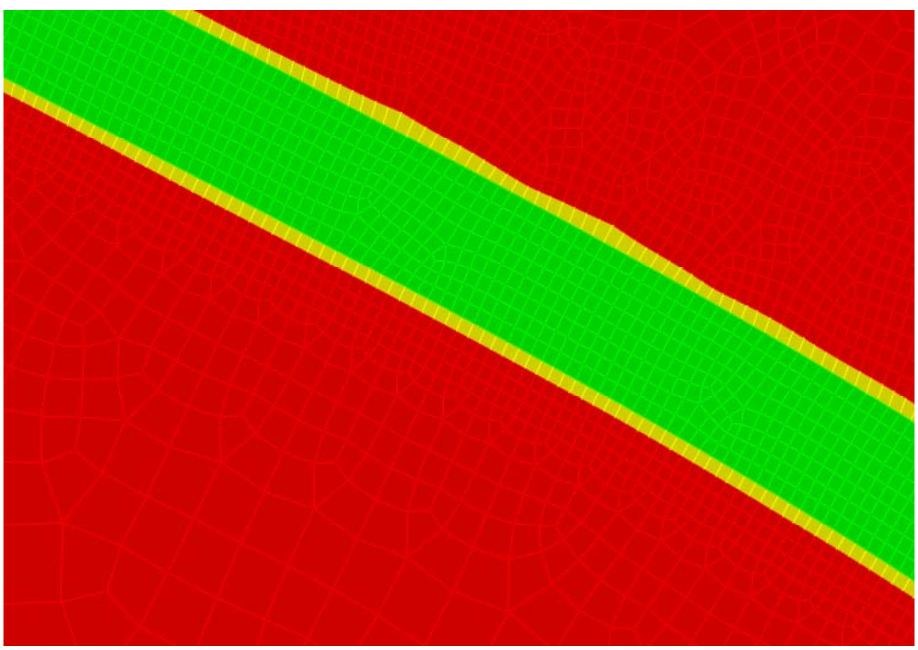

Figure 9 Picture showing a section of the meshed model of the 2D bone/suture structure with an interphase, shown in yellow, between the bone and suture.

2D Model of the Cranium

Stress tensors in the YY (σ_y), ZZ (σ_z) and YZ (τ_{yz}) directions along the bone/suture interface were obtained. These stress data were then exported to Microsoft Excel where they were used to obtain the maximum principal and shearing stresses along the bone/suture interface.

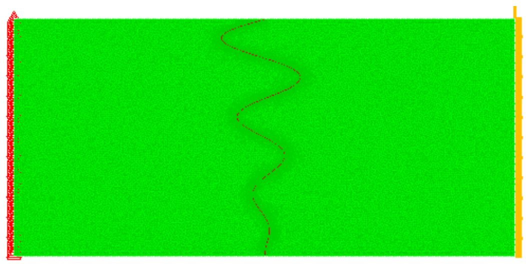

Model with 0.01mm width suture

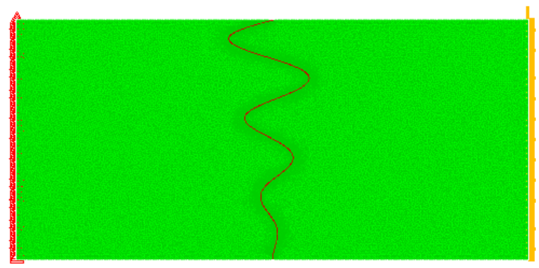

Model with 0.02mm width suture

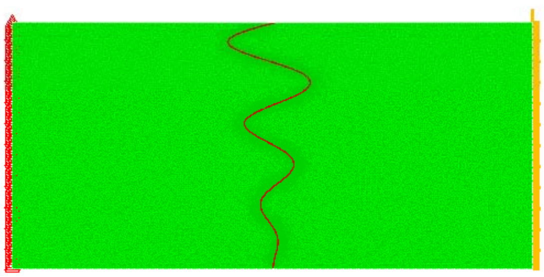

Model with 0.03mm width suture

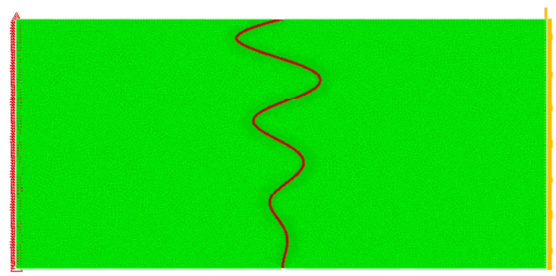

Model with 0.04mm width suture

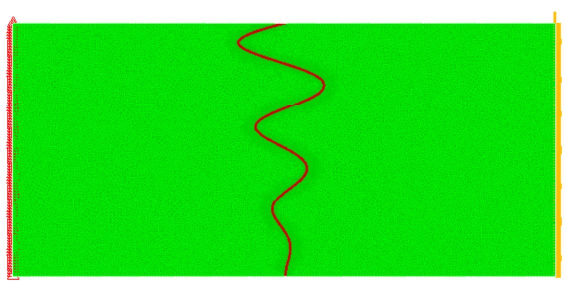

Model with 0.05mm width suture

Figure 10 Showing 2D models with various widths of suture ranging from 0.01mm to 0.05mm.

To help visualize pictorially the distribution of the stresses along the wavy pattern of the suture, a plot of the maximum principal and shearing stresses (Figure 11 and Figure 12) along both upper and lower bone/suture interfaces were obtained. From Figure 11 it is clear that at the advancing peaks (convex sides) and receding valleys (concave sides) the stress decreases as the amplitude of the suture pattern increases. This pattern is consistent with both the upper and lower interfaces of the suture. Stresses at valley locations are generally higher than stresses at peak locations and stresses in between peaks and valleys are the highest. Also as wavy amplitude increases the stress variation increases compared to the relatively flat level at the beginning.

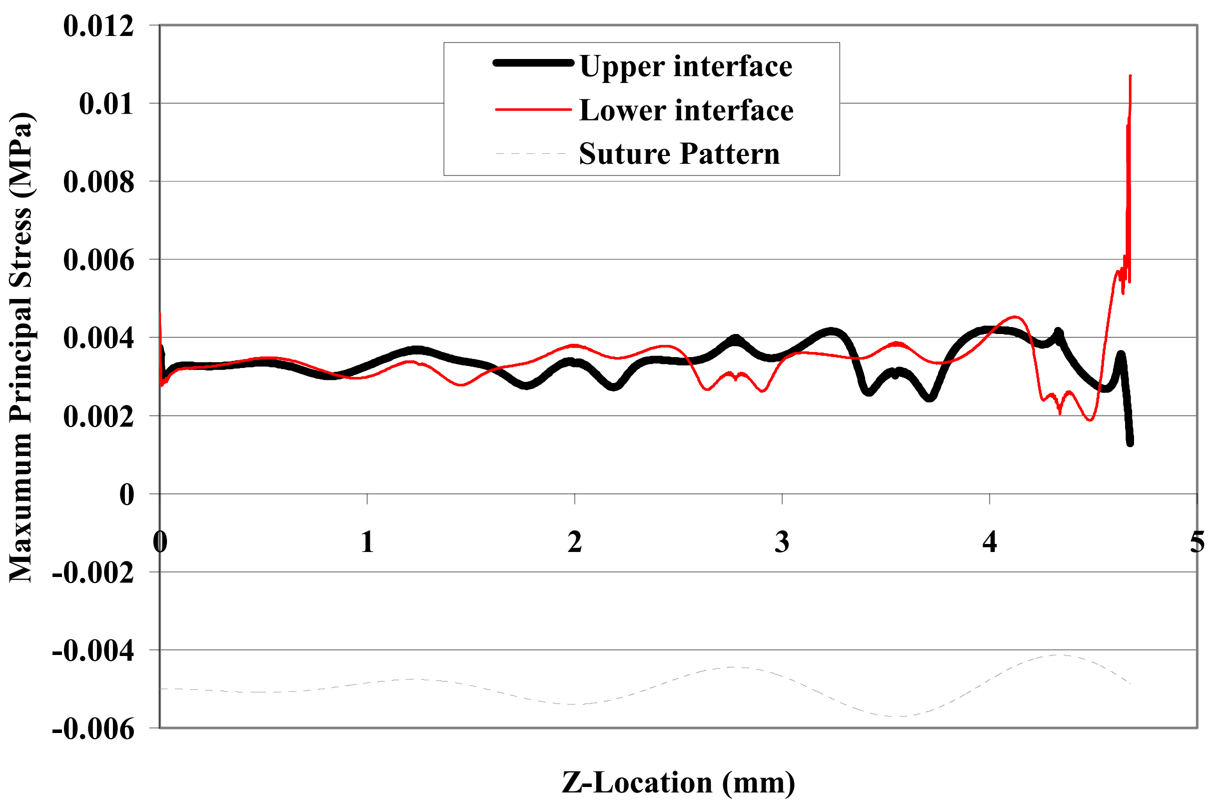

Figure 11 Variation of the maximum principal stresses at the bone fronts along the upper and lower interfaces for uniform width.

Figure 12 show plots of maximum shearing stresses. The shearing stress reaches its maximum at the valley locations and it increases as the amplitude of the wavy suture increases, but it shows lower stress level and less fluctuation in between the peaks and valleys. The stresses reach its lows at peak locations.

Mohr's circles were also constructed to provide a graphic interpretation of the general stress behavior along the bone/suture interfaces (Figure13). The diameter of the circles shows the magnitude of the shearing stresses and the intercepts of the horizontal axis (stress axis) with the circle, shows maximum or minimum principal stresses with a positive intercept (positive region is to the right of the origin which is the intersection of the shear and stress axis) being tension and a negative being compression.

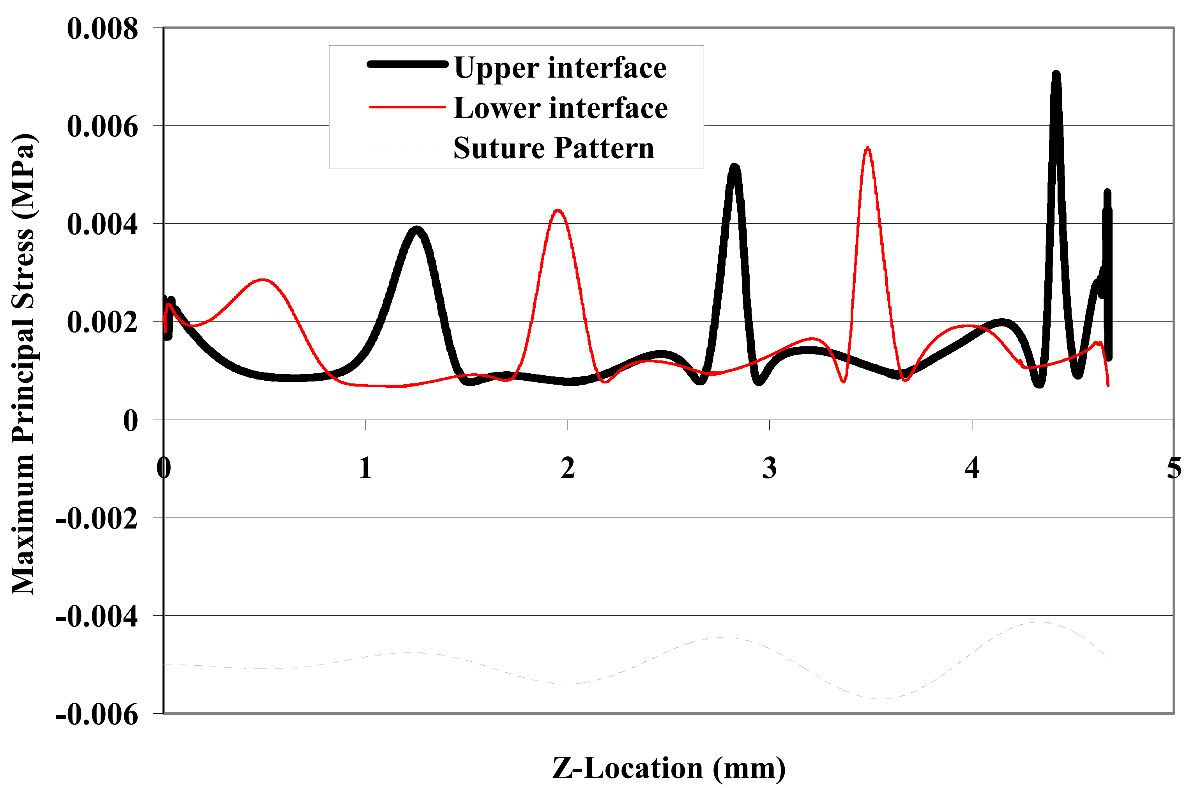

Figure 12 Variation of the maximum shearing stresses at the bone fronts along the upper and lower interfaces.

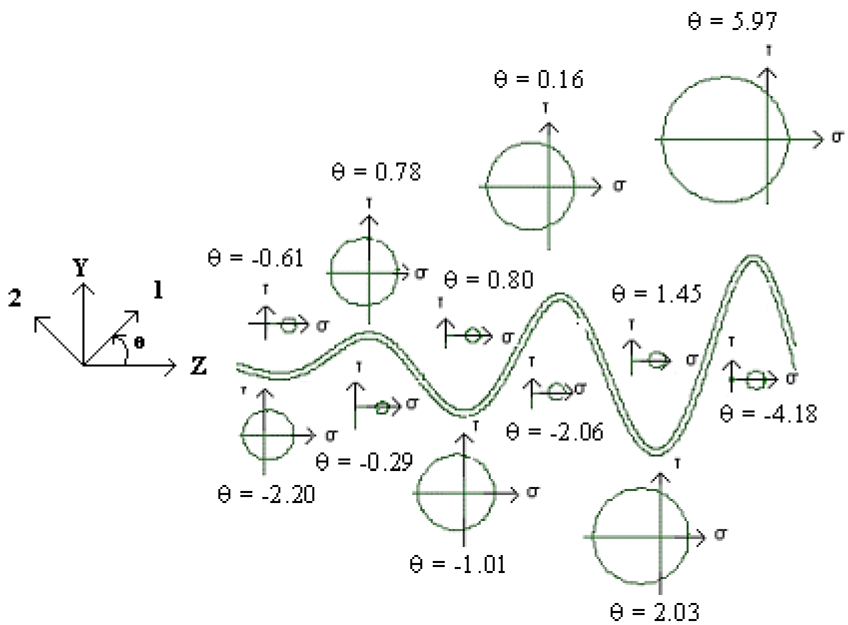

Figure 13 Mohr's circles drawn along the bone/suture interface for the 2D model.

Figure 13 show that the shear stresses at the valley locations on both the upper and lower interfaces increase as the amplitude of the suture increases. Also the normal stresses at the valley locations are biaxial tensile-compressive with an increase in the compressive stress and decrease in tensile stress as the amplitude of the suture increases. Clearly the circles shift to the left as the amplitude of the suture pattern increases causing the drop in tensile stress. The peak locations have small shear stresses with normal stresses that are entirely tensile (biaxial tension).

Biologically shear stresses cause bone resorption and tension causes bone formation. Correlating these results and the biological behavior of bones suggests that the high shear stresses coupled with the biaxial tensile-compressive stresses at the receding valleys may result in bone resorption. Furthermore, the biaxial tensile stresses with small shear at the advancing peaks results in bone formation. As the magnitude of these stresses increases or decreases (with increasing amplitude of wavy suture pattern) bone formation or resorption also increases which suggests a mechanism of suture interdigitation. This mechanism may however be driven by the high shear and biaxial tensile-compressive stresses since the change in the biaxial tensile stress with its accompanying small shear do not vary much.

Model with Interphase between the Bone and Suture

For the model with interphase normal and shear stresses in the YY, ZZ and YZ directions along the interphase suture interface were obtained. These values were then used to obtain the maximum principal and shearing stresses along the interphase suture interface. The values of the principal stresses at the peak and valley locations were used to plot Mohr's circles as shown in Figure 14.

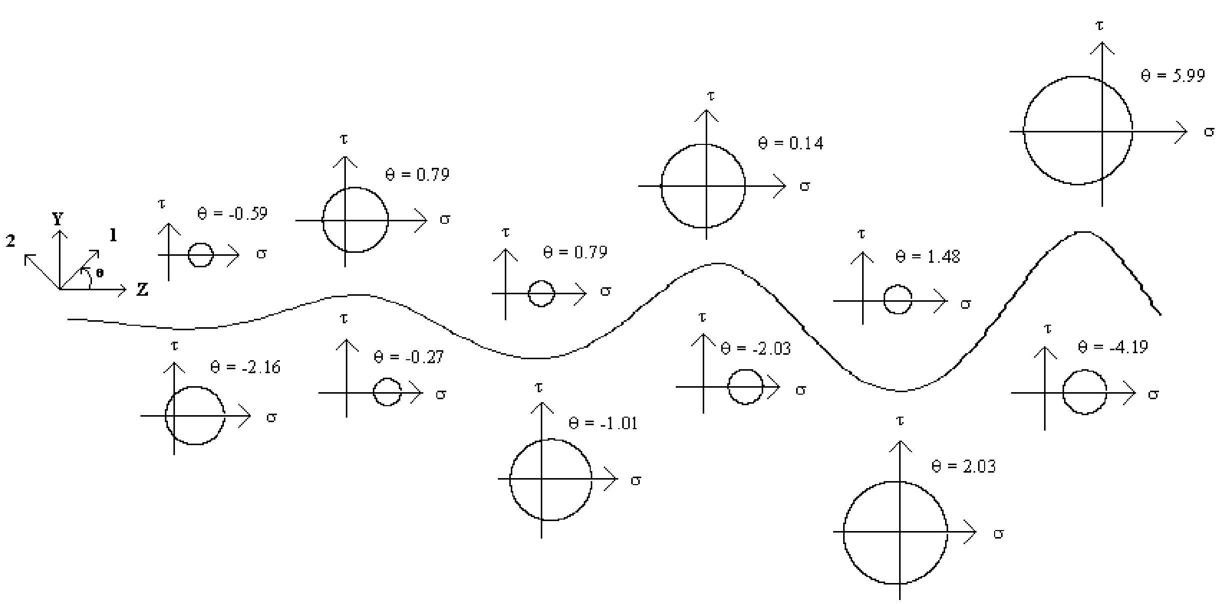

Figure 14 Mohr's circles drawn along the interphase suture interface for the model with interphase. Note the similarities in pattern compared to Figure13.

At receding valleys on both the upper and lower interfaces, the diameter of the circles (hence the magnitude of the shear stresses) increases as the amplitude of the wavy suture increases. Also at this same locations the normal stresses are biaxial tensile-compressive with increasing compressive stresses and decreasing tensile stresses as the waviness of the suture pattern increases. At the advancing peaks for both the upper and lower interfaces, there is a negligible increase in the magnitudes of the normal stresses (biaxial tension) and a small increase in the shear stresses as the amplitude of the pattern increases. Comparing these results from Figure 14 with Figure 13 it is clear that there is not much difference in the sizes and shifting of the circles. Observing closely the tensile stresses at the receding valleys shows that they are slightly higher than the tensile stresses in the model without an interphase. This is indicated by the circles shifting a little more into the positive region of the σ axis as shown in Figure 14. This slight increase in the tensile stresses at the receding valleys may be due to the introduction of the interphase, which has material properties different from that of bone. Even so, the results still suggest that there is bone resorption at receding valleys and bone formation at the advancing peaks.

Simulation of Suture Fusion

To help visualize the changes in the stress states at the interface during the process of fusion, Mohr's circles were plotted. The Mohr's circles were plotted for all the five different suture widths at the same location (highest peak of the wavy suture pattern) on the bone/suture interface for the lower and upper interface (Figure 15). For the 0.05mm width suture the shear stress on the lower interface is bigger than the upper interface. Also the normal stresses on both interfaces are biaxial tensile with the maximum principal stress on the lower interface larger than the upper interface. For the subsequent suture widths the stress states at the lower interface are higher than the upper interface. This difference gradually reduces as the suture width decreases. It is clear that for the 0.02mm and 0.01mm width sutures, the stress states are almost the same.

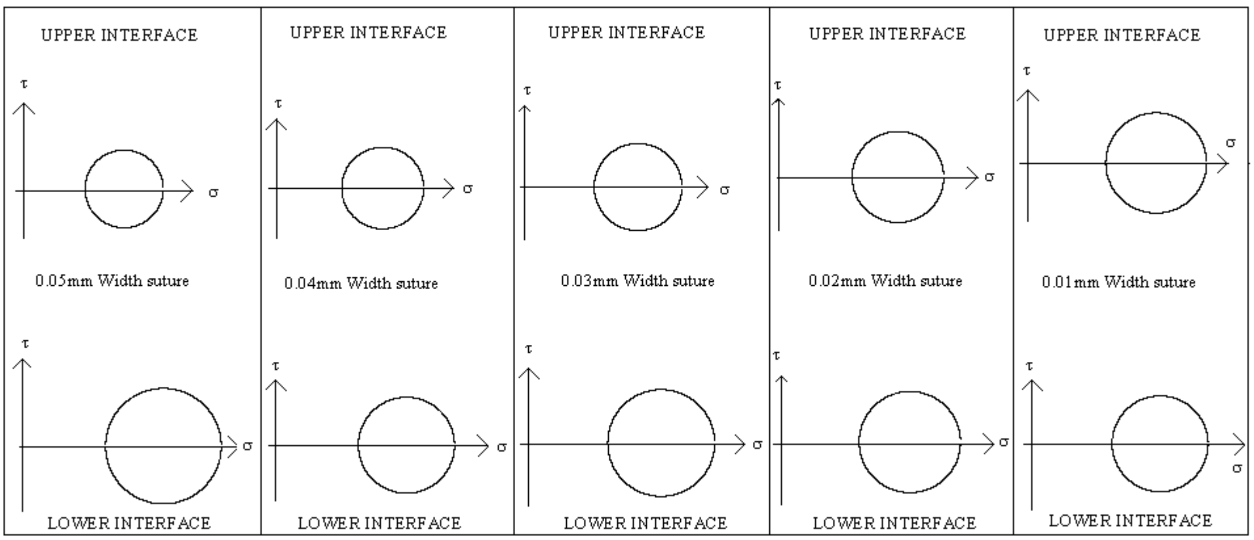

Figure 15 Mohr's circles at the same location on the bone/suture interface showing the sizes of the circles on the lower and upper interfaces becoming the same as the width of the suture decreases.

That is the high biaxial tensile stresses and the shear stresses are almost the same. Since high shear stresses biologically result in bone resorption and high normal stresses result in bone formation, there would be neither bone formation nor resorption when the stress states at the upper and lower interfaces are the same. It is interesting to note that from Figure 13 and Figure 14, where the suture width is 0.15mm, the stress state at the upper interface is biaxial tensile-compressive with high shear stress and that on the lower interface is biaxial tensile with small shear. This shows that as the suture width decreases the biaxial tensile-compressive stress state at the upper interface falls out of the compressive region and becomes entirely tensile and the shear stress on the lower interface increases. This mechanism continues until the biaxial tensile stresses and shear stresses on both interfaces become equal at which stage there will be neither bone formation nor resorption, hence fusion.

Also stress values along the bone/suture interface were obtained from which plots of the maximum principal stresses along the suture were obtained for all five models (Figures 16 and 17). The plots show that as the suture width decreases the difference in the magnitude of the maximum principal stresses on both the upper and lower interfaces decreases. Also the difference in the maximum principal stresses from the Mohr's circles in Figure 15 decreases as the suture width decreases. This results therefore confirms the results from the Mohr's circles in Figure 15.

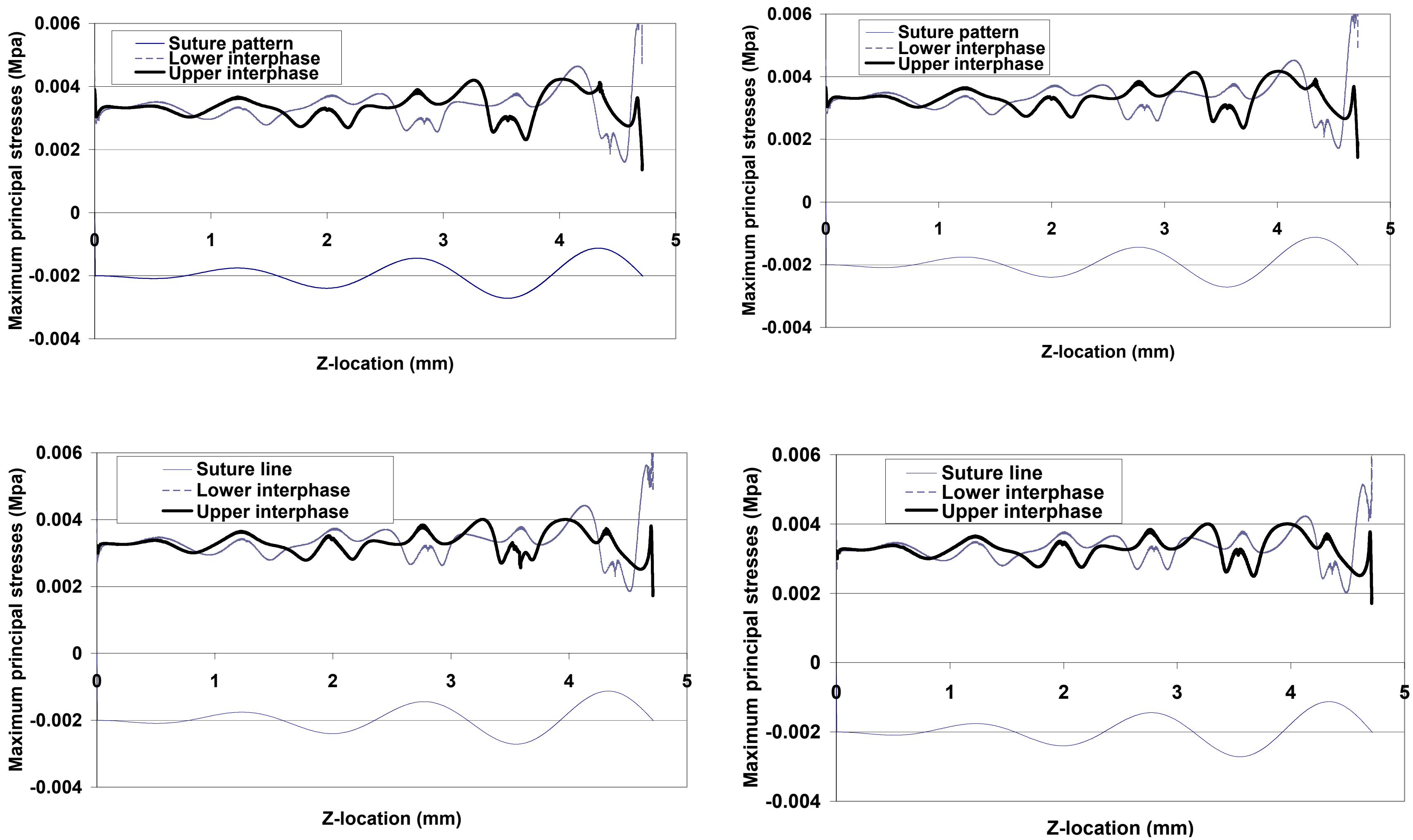

Figure 16 Plots of maximum principal stresses along the upper and lower interfaces of the different widths of suture with the top left showing plot for suture with 0.05mm width; top right, suture with 0.04mm width; bottom left, suture with 0.03mm width and bottom right suture with 0.02mm width.

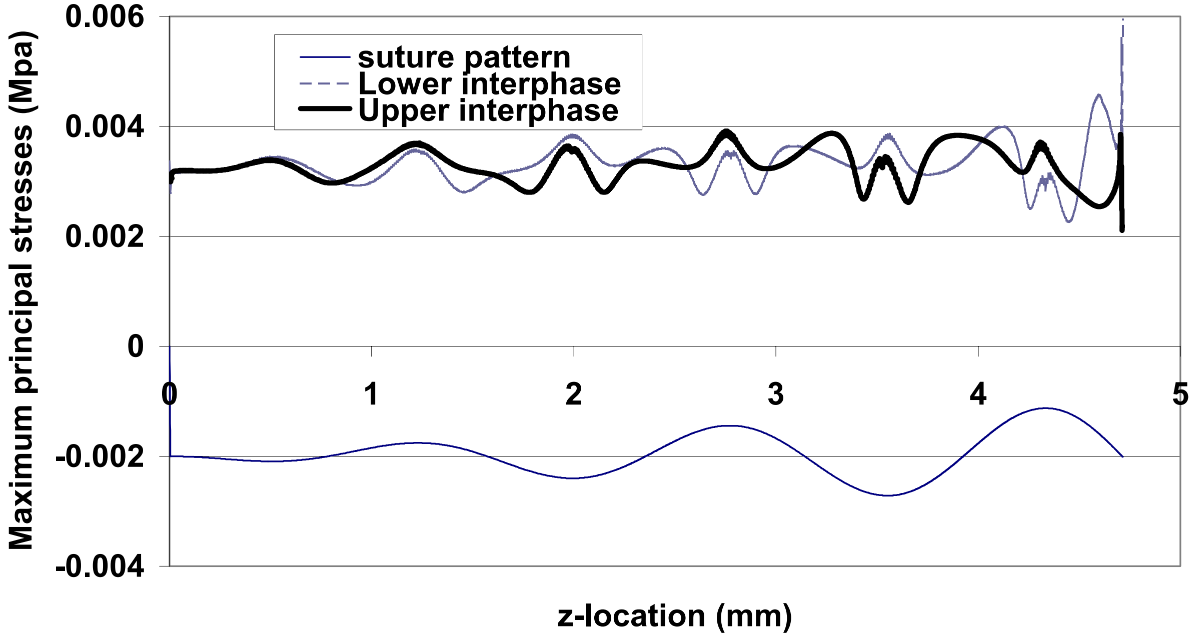

Figure 17 Plot of maximum principal stresses along the suture for suture with 0.01mm width.

CHAPTER 5

THE EFFECT OF NONLINEARITY OF BONE ON THE STRESS DISTRIBUTION AT THE BONE/SUTURE INTERFACE

Modeling Considerations

A nonlinear study was performed in which the true stress strain curve for bone was used. Data for the true stress strain curve (Figure 18) was obtained from Porter (2004). The obtained data was entered under the material properties for bone in the FEA program.

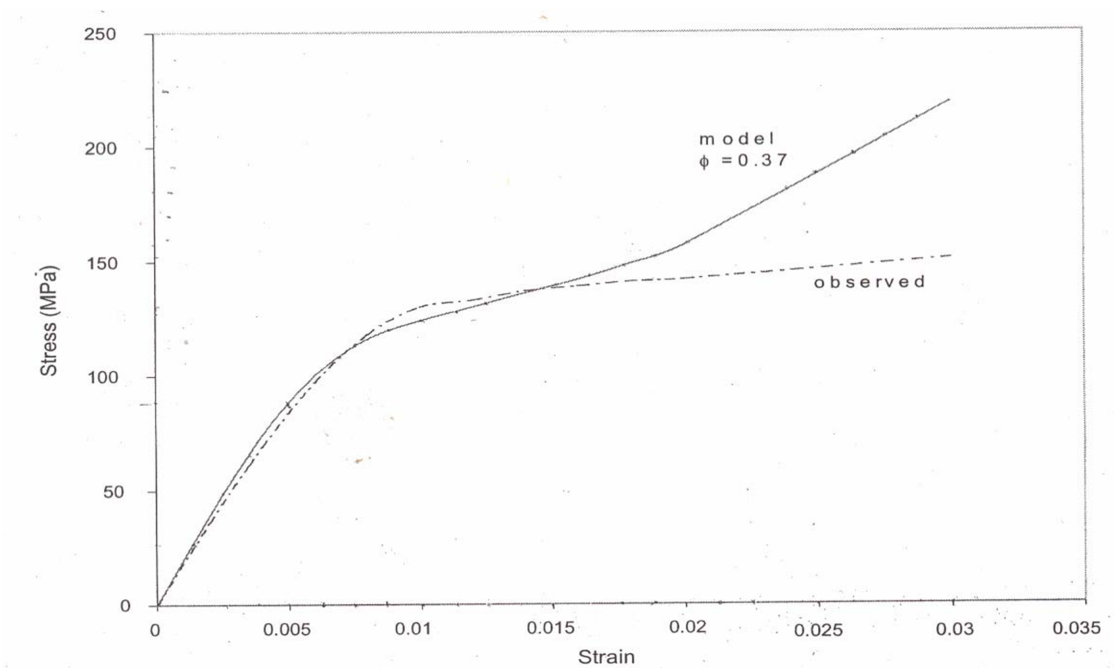

Figure 18 Predicted stress-strain profile of human bone (solid line) compared with experimental data (dashed line) (Porter, D, 2004).

The first data point of zero stress/zero strain was not entered due to the iterative nature of calculation of the modulus of elasticity from point to point. An elastic modulus of 8.42 GPA and a Poisson ratio of 0.28 for bones were entered. The suture was treated as an isotropic material with a modulus of elasticity of 50 MPA and a Poisson ratio of 0.4. The model was fixed at one end and a negative surface load of 3.33KPa was applied at the other end to induce tension. Another analysis was performed in which the model was loaded with a surface load of 24MPa. The yield stress of bone is about 50MPa and loading the model with 24MPa produced yielding in the model especially along the highest peak of the bone/suture interface. So the 24MPa load was used to obtain yielding in the model to demonstrate the nonlinear behavior of bone. For the analysis type, MES (Mechanical Even Simulation) with nonlinear material models was chosen. For the analysis parameters a load curve with initial load of zero, which is ramped up linearly to the applied load, was used. Also a duration of one second and time step of 100 was used. The analysis for the model was then run and the results analyzed.

For the sake of comparative analysis a linear analysis was also performed on the model using a surface load of 24MPa.

Effect of Nonlinear Analysis

From the nonlinear study in which 24MPa load was applied, the node on which the highest stress occurred was selected and the stress against time step curve obtained (Figure 19). A linear curve from the linear analysis was constructed alongside the nonlinear curve (Figure 19). From the curves, it is clear that the nonlinear curve starts to deviate from the linear curve at a stress of about 50MPa. From Figure 18 yielding starts from about 50MPa and this indicates that the bone is in the nonlinear region.

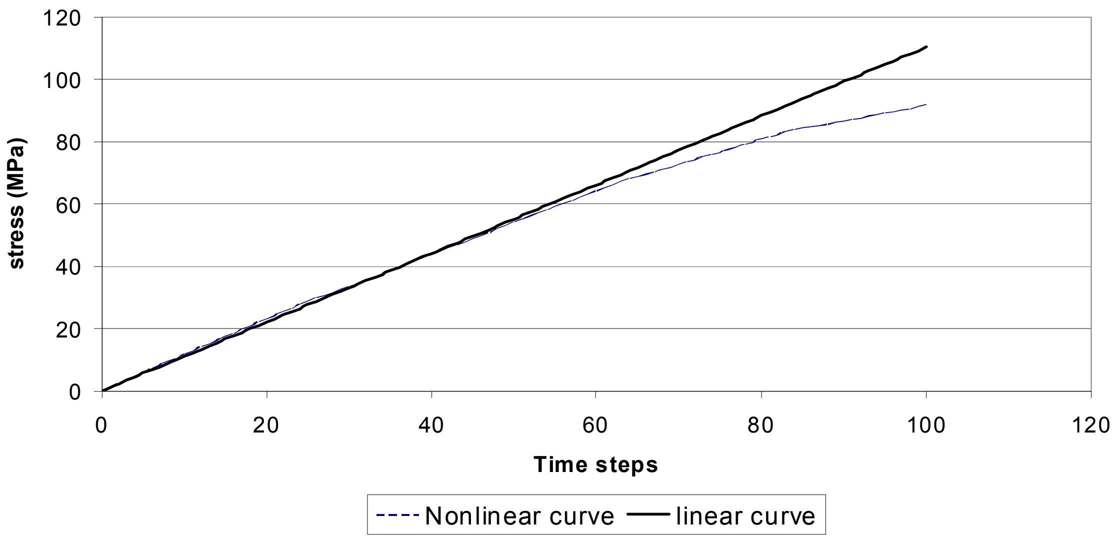

Figure 19 Plot of stress against time steps for linear and nonlinear analysis using the true stress strain curve for bone as the material properties for bone.

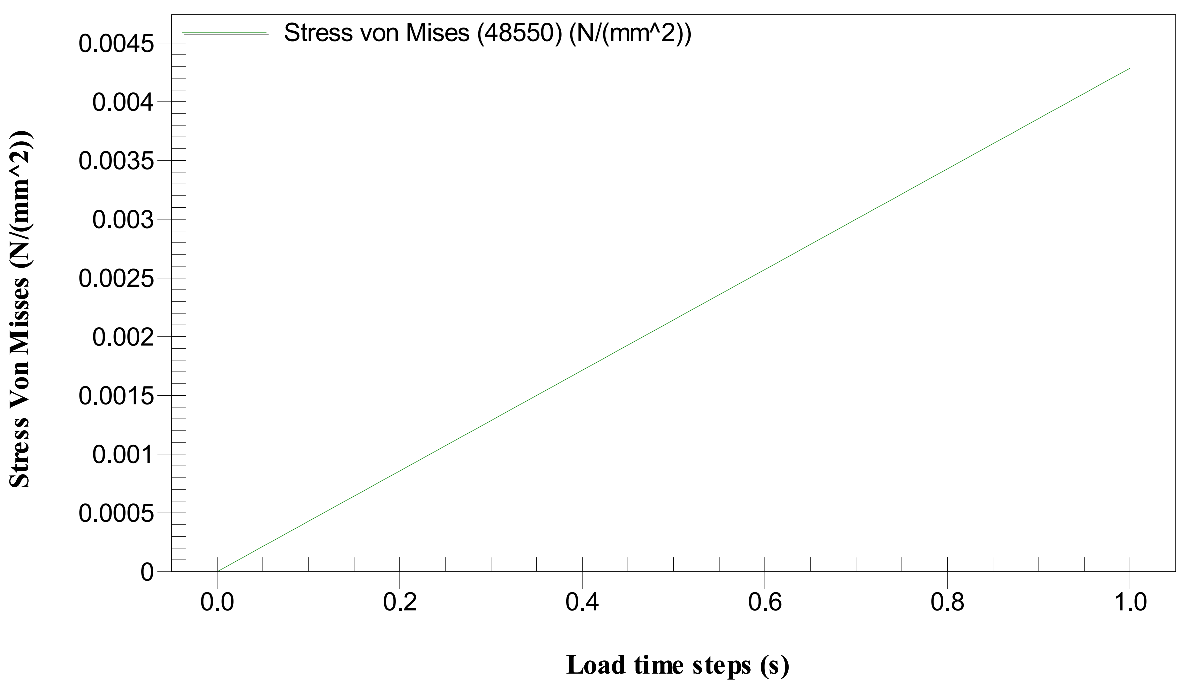

Figure 20 A nonlinear curve obtained by plotting Von Misses stress against time duration.

For the nonlinear study in which 3.33KPa was used, the highest stress was selected and the plot of the Von Misses stress against the time duration on this node was obtained as shown in Figure 20. The highest stress was near to the bone/suture interface at a location where the amplitude of the suture was highest. From the plot the highest stress is about 4.5KPa, which is much less than the yield stress of about 50MPa. This shows that with the loading considered in this study, the bone is still in the linear region. Therefore despite the fact that bone is a nonlinear material nonlinearity is not a concern under the applied load of 3.33KPa.

CHAPTER 6

THREE DIMENSIONAL FINITE ELEMENT STUDY OF THE STRESS DISTRIBUTION AT THE BONE/SUTURE INTERFACE

Modeling Considerations

The 3D model was created using Proengineer Wildfire 2.0 (ProE), a CAD software program. In proE the top view of the cranium was sketched. After sketching, the resulting geometry was extruded to a depth of about 12cm. This resulted in a 3D solid structure that was trimmed into the shape of the cranium. Material from the bottom surface of the 3D solid structure was removed to a wall thickness of about 0.5mm. This resulted in a 24mm by 17mm by 6mm 3D structure of the cranium with a wall thickness of 0.5mm(Figures 21 and 22). To add the sutures to the model of the cranium, a sketch of the sagittal suture was imported from ALGOR into ProE. In ProE the sketch of the coronal and lambdoid sutures were added to the sagittal suture. The complete sketch was then extruded to the thickness of the cranium. The resulting 3D solid of the sutures was then used to cut through the 3D model of the cranium, choosing to preserve the part that the cut removed. This process was repeated but the part that the cut did not remove was preserved. This resulted in a 3D cranial model without sutures and a model of the sutures. The two models were then put together to form an assembly model of the cranium. The resulting model was then transferred to ALGOR, where it was surface meshed and eventually solid meshed. Brick and tetrahedron elements were used for the solid meshing. This meshing process generated 95,312 elements with a mesh size of 0.641712 for the cranial bones and 9959 elements with a mesh size of 0.11064 for the cranial sutures. To ensure stress continuity at the bone/suture interface, the mesh sizes in the neighborhood of the interface were refined. The model was then grouped into 5 parts and 3 surfaces. The parts were the frontal bone, two parietal bones, the occipital bone and the cranial sutures. The inner surface of the model was assigned a surface number to enable the application of surface pressure and the area at the base of the cranium was also given a different surface number to enable the application of boundary conditions. The model was then transferred to the FEA interface of ALGOR. Here element types, material properties, loads and constraints were assigned to the model. Bricks were assigned as the element type and material properties for bone was 17300MPa for the Modulus of elasticity (E), 0.28 for Poisson ratio (ν) and 6760MPa for shear modulus of elasticity (G). For the suture an $E = 50$MPa, $\nu = 0.45$ and a $G = 17.34$MPa was assigned.

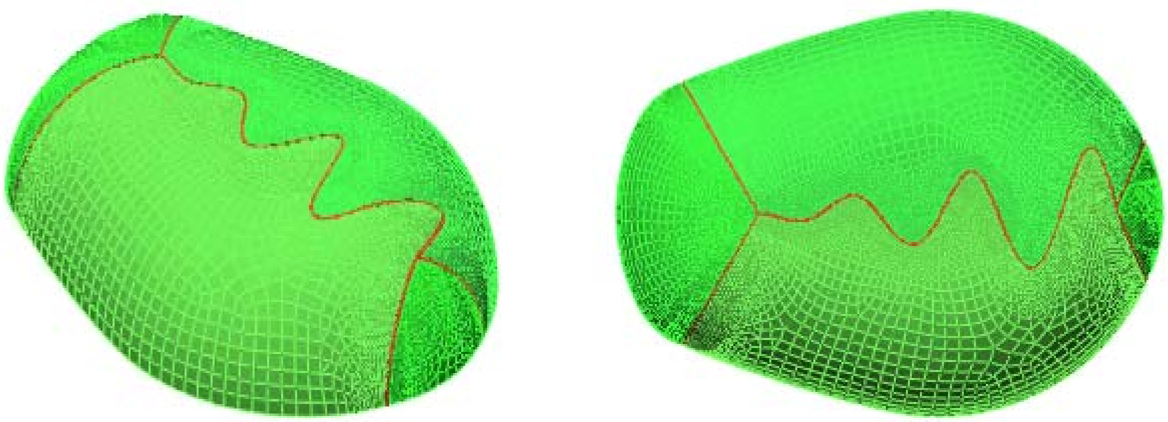

Figure 21 Left: Isometric view of the 3D cranial model. Right: Top view of the 3D cranium.

The base of the cranial model was fixed and a surface pressure of 1.33KPa was applied to the interior surface of the cranium. To model an infant skull the model for the adult cranium was scaled down to half its size.

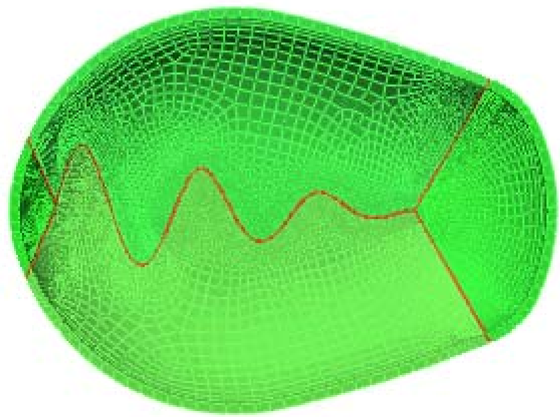

Figure 22 Bottom view of the 3D cranial model showing cranial bones in green and cranial sutures in red .

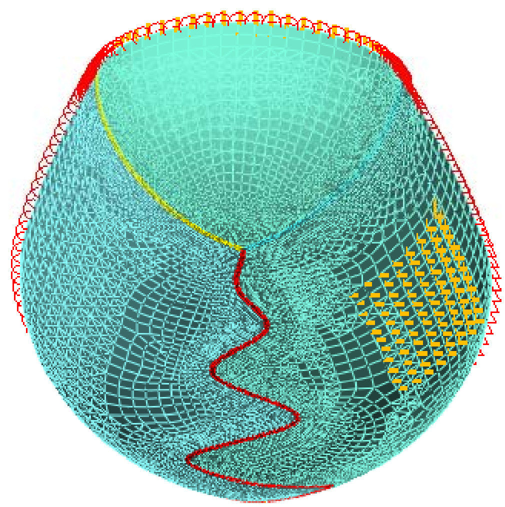

Figure 23 3D model of the cranium showing pressure loading to the medial-lateral side to simulate the loading condition in multiple birth syndrome.

The eventual size was 12mm by 8.5mm by 3mm with a wall thickness of about 0.25mm assigned to the sutures. Also an intracranial pressure value of 373.3Pa (Henderson, J.H et al., 2002) was also used. The resulting model was prepared as in the adult model but infant material properties were applied to the bone and sutures. E = 3300MPa, ν = 0.38 and a G = 1179MPa were assigned to the bone and a E = 10MPa, ν = 0.45, a G = 3.33 MPa were assigned to the suture.

To simulate multiple birth syndrome (MBS) and the stress put on the cranium during chewing, a surface pressure of 200KPa was applied to the medial lateral side of the parietal bone of the adult cranium (Figure 23).

To simulate the various types of synostosis the suture was divided into five parts. The parts were the two coronal sutures, the sagittal suture and the two lambdoid sutures. The whole model was then solid meshed and prepared as before. For the various kinds of synostosis, the suture to be fused was assigned the properties of bone while the others remained patent (no ossification). Static stress with linear material model analysis (linear analysis) was performed on the adult, infant, multiple birth syndrome and the various types of synostosis models.

Adult Cranium

In ALGOR, the stresses in the model were analyzed as follows. Figure 24 showing the contour plots of stresses in the cranium after load was applied indicates that there are high stresses at the peaks and valley location of the sagittal suture. Also high stresses exist at the top section of the model. The picture of the deformed model was obtained (Figure 24) and from this picture it can be seen that the interlocking parietal bones tend to shift up or bulge when load is applied. This shifting or bulging stretches the outer surface of the sagittal suture and shortens the inner layer. In other words it puts tension on the outer surface of the sagittal suture and compression on the inner surface. The last third of the sagittal suture seems not to have undergone much shifting or bulging because of its curvature, which allows it to better resist the stress. Isolating the sagittal suture and obtaining its deformed and undeformed shape (Figure 25), it is observed that the top section of the suture deforms more than the inner section.

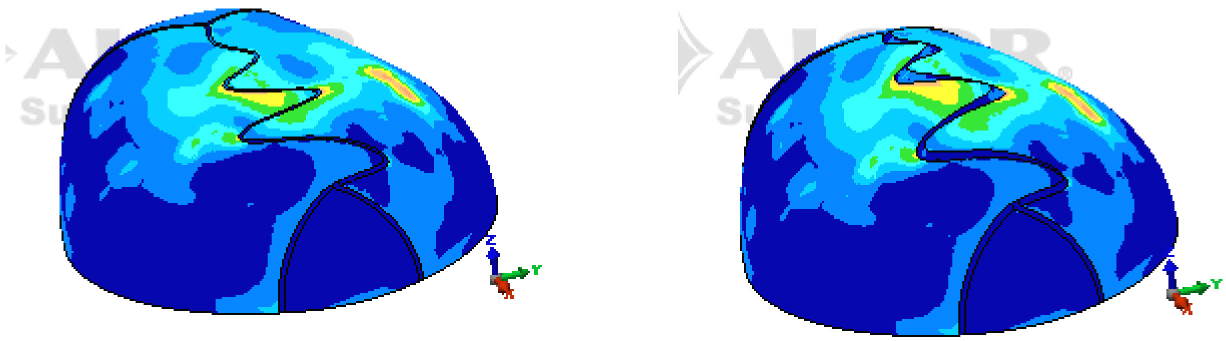

Figure 24 Contour plot of the stress distribution in the undeformed model, right and deformed model, left.

In ALGOR the maximum principal stress, intermediate principal stress and minimum principal stress values along the sagittal suture parietal bones interface were obtained. There are three planes on which the maximum, intermediate and minimum principal stresses act, these are the 2.3, 1.3 and 1.2 planes. The maximum and minimum principal stresses act on the 2.3 plane, the maximum and intermediate principal stresses act on the 1.3 plane and the intermediate and minimum principal stresses act on the 1.2 plane. The values of these stresses at the peaks and valleys positions of the parietal bone/sagittal suture interface were used to plot 3D Mohr's circles (Figure 26 to Figure 30). To capture the stress states along the depth of the suture interface, the model was meshed in such a way as to produce layers of elements on the bone/suture interfaces.

Figure 25 Contour plot of the stress distribution in the undeformed model of the sagittal suture, left, contour plot of the stress distribution in bottom view of the deformed model of the sagittal suture, middle and contour plot of the stress distribution in the top view of the deformed model of the sagittal suture.

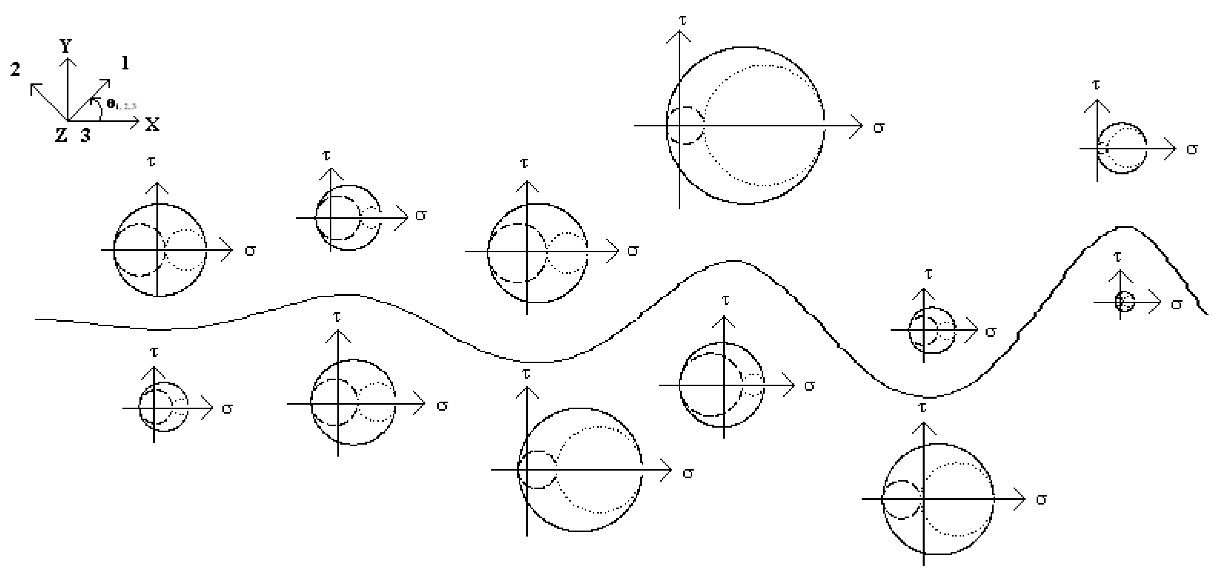

Figure 26 3D Mohr's circles of stresses (dotted circles = stresses on 1.3 plane, short dash circles = stresses on 1.2 plane, continuous circle = stresses on 2.3 plane.) at peak and valley locations along the sagittal suture on layer one. See appendix for orientations of principal stresses.

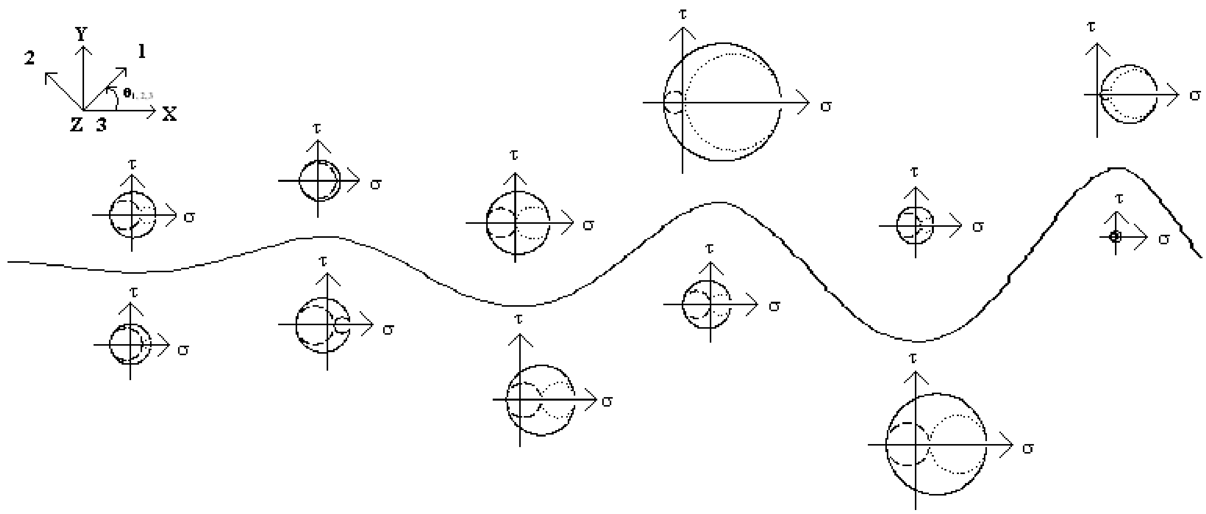

Figure 27 3D Mohr’s circles of stresses (dotted circles = stresses on 1.3 plane, short dash circles = stresses on 1.2 plane, continuous circle = stresses on 2.3 plane.) at peak and valley locations along the sagittal suture on layer two. See appendix for orientations of principal stresses.

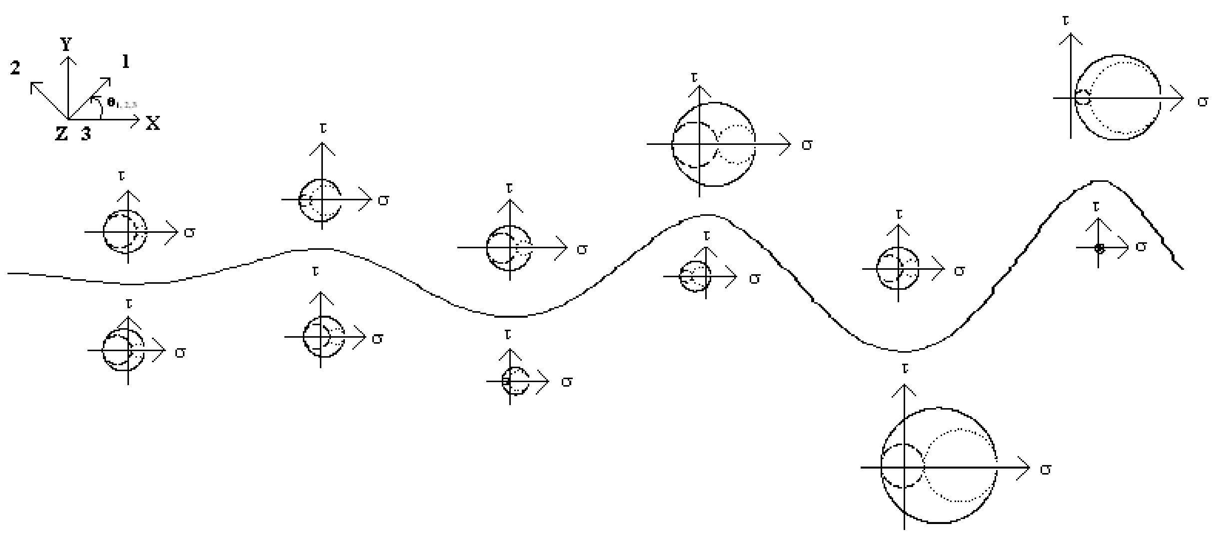

Figure 28 3D Mohr’s circles of stresses (dotted circles = stresses on 1.3 plane, short dash circles = stresses on 1.2 plane, continuous circle = stresses on 2.3 plane.) at peak and valley locations along the sagittal suture on layer three. See appendix for orientations of principal stresses.

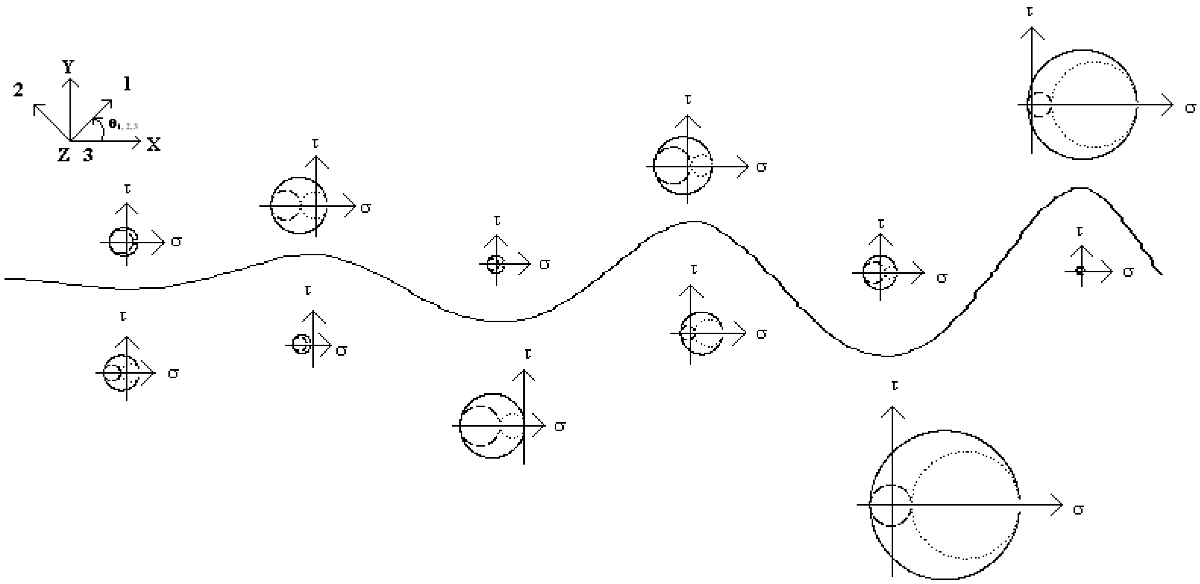

Figure 29 3D Mohr's circles of stresses (dotted circles = stresses on 1.3 plane, short dash circles = stresses on 1.2 plane, continuous circle = stresses on 2.3 plane.) at peak and valley locations along the sagittal suture on layer four. See appendix for orientations of principal stresses.

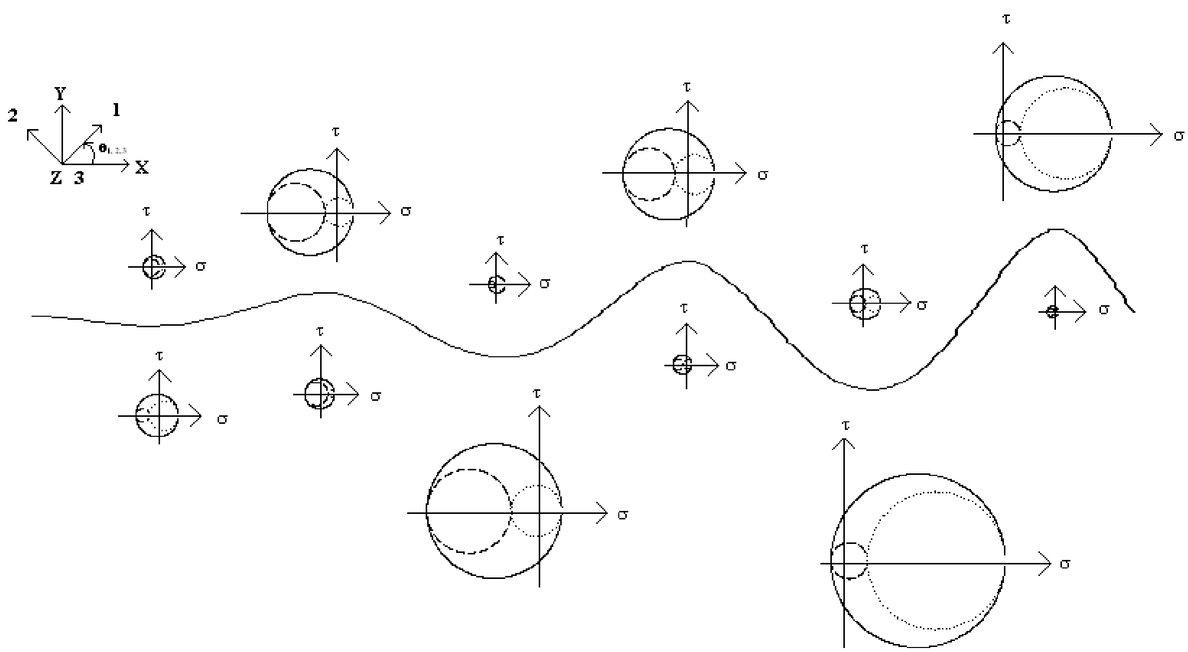

Figure 30 3D Mohr's circles of stresses (dotted circles = stresses on 1.3 plane, short dash circles = stresses on 1.2 plane, continuous circle = stresses on 2.3 plane.) at peak and valley locations along the sagittal suture on layer five. See appendix for orientations of principal stresses.

The interface therefore had five layers on which stresses act and so plots of the Mohr's circles were obtained for each of these layers. The layers were numbered one through five with one being the outermost layer, which corresponds to the outer surface of the 3D cranium, and five being the innermost layer which corresponds to the interior surface of the cranial model. The interfaces were the interface of the sagittal suture with the right parietal bone (upper interface) and the left parietal bone (lower interface). Mohr's circle is a pictorial representation of all of the stress components (be it tensile, compressive or shear) at a point. 3D Mohr's circles are circles plotted to represent the stress components that exist on the three planes of a 3D object. The circles on the different planes were analyzed separately to ascertain a relation between the stress components on the different planes and the pattern of interdigitation. Also the effect of the stresses on the different planes was also determined.

Towards the end of the sagittal suture, where its wavy pattern reaches its peak (which spans about a fifth of the length of the suture) it is seen that the stresses are different from those experienced in the remaining section. As the earlier section of the suture bulges out, the last fifth section bulges in due to the curvature at that section and the boundary and loading conditions. As a result of this, attention would not be paid to the behavior of the stress states in that section.

Looking at the 3D Mohr's circles drawn for layers one through five on the 2.3 plane (circles with continuous lines) it could be seen that there is a general increase in the shear stress from valley to valley as the amplitude of the sagittal suture pattern increases (Figure 26 to Figure 30). This occurs for both the upper and lower interface. For the peak locations there is not much variation between the magnitudes of the shear stresses and those of the tensile and compressive stress components as the amplitude of the suture pattern increases. This trend is seen in all the layers of the bone sagittal suture interface. Compared to the stresses at the receding valleys, the shear stresses on the advancing peaks are relatively low and the maximum and minimum stresses are biaxial tensile compressive. As stated earlier, high shear stresses induce bone resorption and high tensile stresses induce bone growth. Thus at the receding valleys which has high shear bone resorption occur and at advancing peaks which have normal stresses bone formation occurs.

This trend begins to change from the third to the fifth layer (Figure 28 to Figure 30). On the third layer, the receding valleys of the lower interface sees a reversal in the trend and shear stress becomes smaller as amplitude increases. Stresses at the upper interface stay consistent with the trend. This suggests that the increase in the amplitude of the wavy pattern (bone resorption) is due to stresses on other planes.

For the fourth and fifth layers, on the lower interface, the trend becomes consistent again but the maximum and minimum stresses become more compressive. The more compressive stresses on the inner layers comfirms the earlier conclusion that there are compressive stresses at the bone/suture interface on the inner layer and tensile stresses on the outer layer.

It is interesting to see that on the upper interface of the fourth and fifth layers the shear, maximum and minimum stresses basically stay the same for the receding valleys. This again suggests that the increase in bone resorption on this layer is not due to stresses on this plane. This is so because for an increase in resorption there should be a corresponding increase in shear.

Shear stresses for the first receding valleys for both the upper and lower interfaces are lower than those on the advancing peaks for the first layer. However tensile stresses on the first advancing peaks are higher than those on the receding valleys. The difference between these stresses reduces through the second layer until it becomes almost the same on the third layer. From the fourth to the fifth layer, the trend reverses with the shear stresses becoming higher than that on the advancing peaks for the first receding valleys. Furthermore, tensile stresses on the first advancing peaks are lower than those on the receding valleys for the fourth to the fifth layers. This is interesting since the side with the higher shear stress is expected to experience bone resorption. At the same time the peaks with the higher shear stresses have tensile stresses that are higher than those on the receding valleys. This indicates that the higher normal stresses override the high shear stresses and thus bone formation occurs. At the same location but on layers four and five the shear stress on the receding valley become bigger than those on the advancing peak. Therefore there may be a threshold of shear or normal stress above which bone resorption or formation will occur regardless of the magnitude of normal or shear stress respectively.

For the 1.3 plane (circles with dotted lines) on which the maximum and intermediate principal stresses act, it is observed that from the first to the third layers shear stresses increase as amplitude increases and this occurs at the receding valleys for both the upper and lower interfaces. As with stresses on the 2.3 plane the shear stresses for advancing peaks are relatively the same. On the third layer the shear stresses on the upper interface are almost the same as those on the receding valleys. This shows that on this layer increase in the amplitude may not be necessarily due to the stresses on this plane. It is most likely due to the increase in shear on the 1.2 planes. On the fourth layer the shear stresses on the upper interface drops as the amplitude increases but on the lower interface it increases with increasing amplitude. However on the fifth layer the shear stresses on both interfaces increases as the amplitude of the wavy suture increases. Also the maximum and intermediate principal stresses are entirely tensile in the first and second layers and from the third to the fifth layers the intermediate principal stress becomes compressive. In other words in the first and second layers there is uniaxial tensile stress and from the third to the fifth layers they are biaxial tensile compressive with the intermediate being compressive. This further shows that the inner surface of the suture experiences compressive stress whiles the outer surface experience tensile stress. On the fifth layer the shear stress on the 2.3 plane remains the same as amplitude increases on the upper interface and on the 1.2 plane (circles with dash lines) there is a reduction. The only increase in shear stress is the stresses on the 1.3 plane so it can be said that the increase in the interdigitation pattern on that layer is due to shear stresses on the 1.3 plane.

Observing the stresses on the first and second layers on the 1.2 plane (circles with dash lines) it is seen that there is a decrease in the shear stresses on the upper and lower interfaces as the amplitude increases which is a reversal in the trend seen on the 2.3 and 1.3 planes for the first two layers. The trend is however becomes consistent with those on the other planes on the third and fourth layers where the shear stress increases with increasing amplitude. On layer four almost all the minimum and intermediate stresses are almost compressive and are entirely compressive on the fifth layer.

Infant Cranium

Comparing the 3D Mohr's circles obtained in this case (Figure 31 to Figure 35) on the five layers along the sagittal suture/parietal bones interface to those obtained from the adult case, it is observed that the pattern of stress distribution remains the same. Also there is not much variation in the magnitudes of the shear, maximum, intermediate and minimum stresses. In effect these results also depict that the sutures wavy pattern is a result of stresses on all three planes. This result was however not expected since it was believed that the changes in the material properties of the bone with age would have an effect on the stress states at the bone/suture interface.

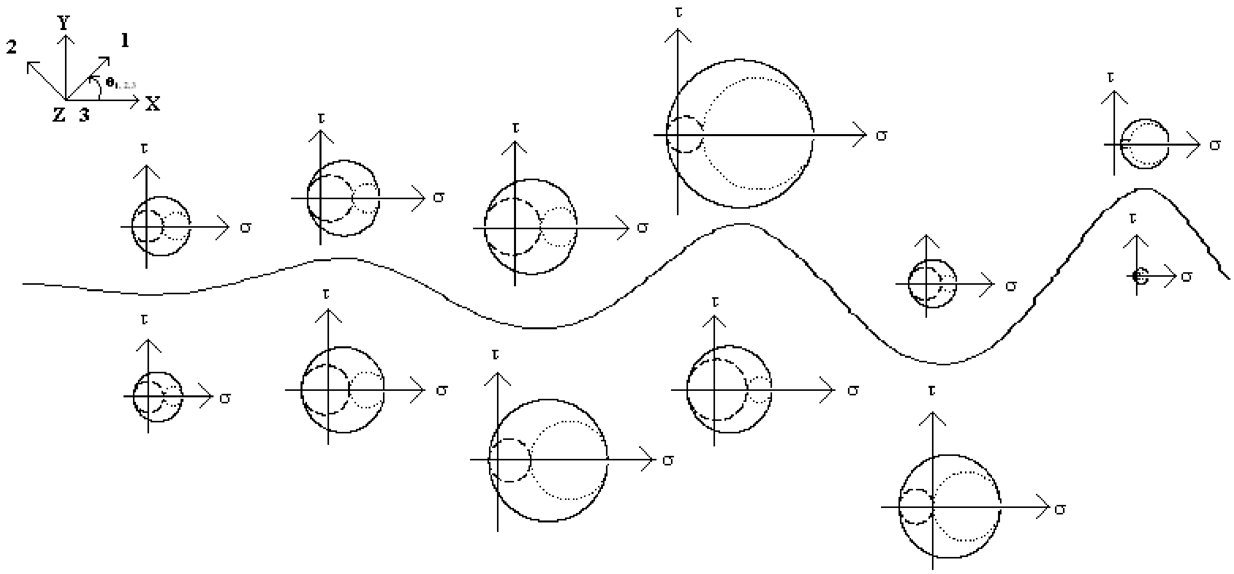

Figure 31 3D Mohr's circles of stresses (dotted circles = stresses on 1.3 plane, short dash circles = stresses on 1.2 plane, continuous circle = stresses on 2.3 plane.) at peak and valley locations along the sagittal suture on layer one. See appendix for orientations of principal stresses.

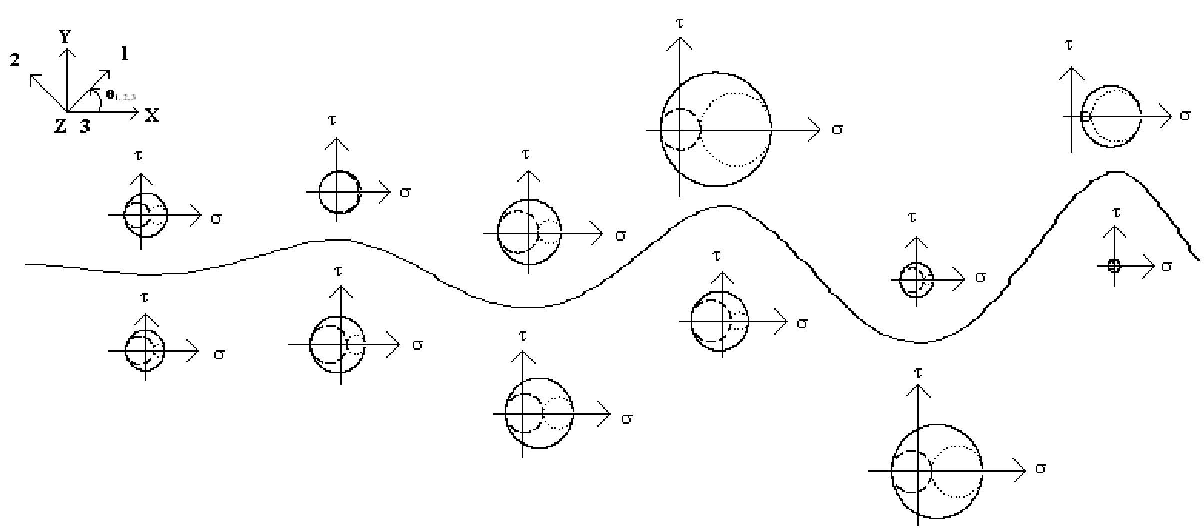

Figure 32 3D Mohr's circles of stresses (dotted circles = stresses on 1.3 plane, short dash circles = stresses on 1.2 plane, continuous circle = stresses on 2.3 plane.) at peak and valley locations along the sagittal suture on layer two. See appendix for orientations of principal stresses.

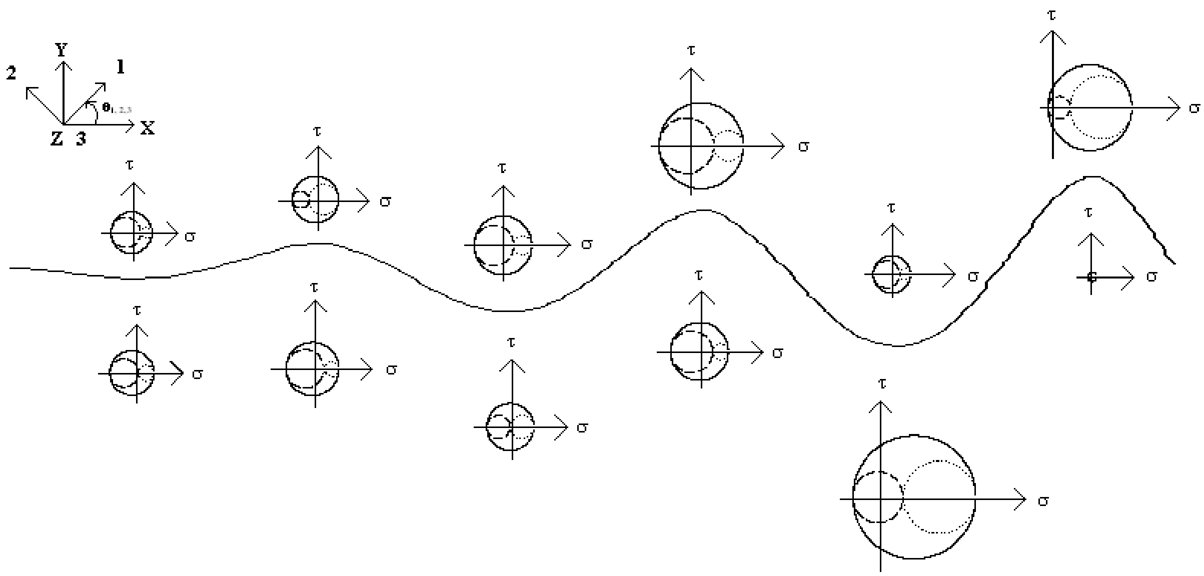

Figure 33 3D Mohr's circles of stresses (dotted circles = stresses on 1.3 plane, short dash circles = stresses on 1.2 plane, continuous circle = stresses on 2.3 plane.) at peak and valley locations along the sagittal suture on layer three. See appendix for orientations of principal stresses.

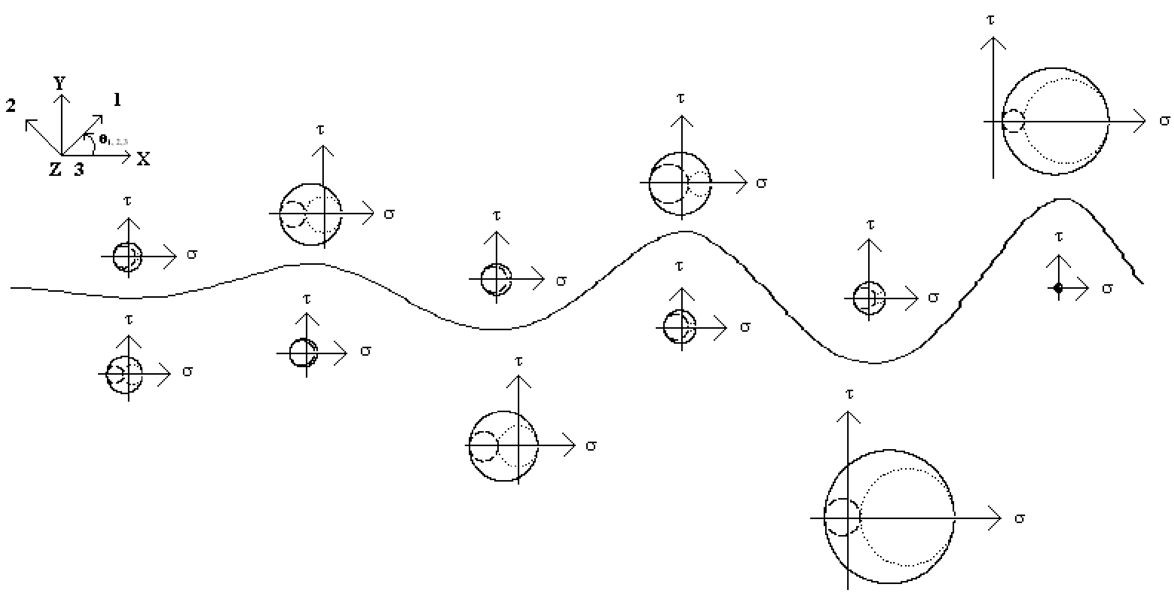

Figure 34 3D Mohr's circles of stresses (dotted circles = stresses on 1.3 plane, short dash circles = stresses on 1.2 plane, continuous circle = stresses on 2.3 plane.) at peak and valley locations along the sagittal suture on layer four. See appendix for orientations of principal stresses.

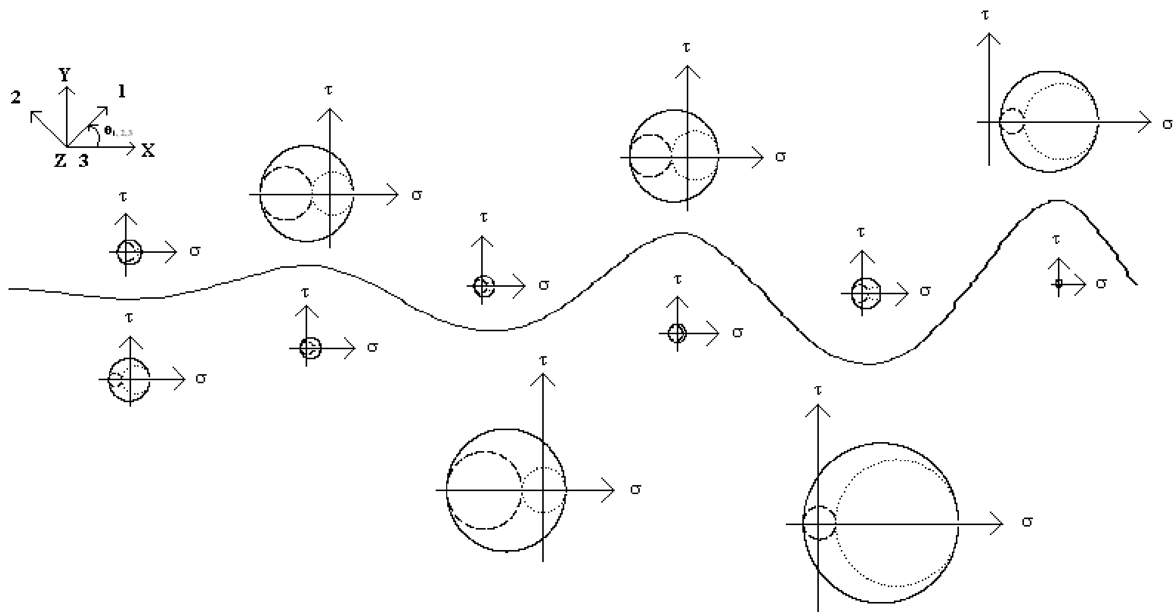

Figure 35 3D Mohr's circles of stresses (dotted circles = stresses on 1.3 plane, short dash circles = stresses on 1.2 plane, continuous circle = stresses on 2.3 plane.) at peak and valley locations along the sagittal suture on layer five. See appendix for orientations of principal stresses.

Multiple Birth Syndrome

From Figure 36, it can be seen that there is a dent at the location where the surface pressure was applied. Comparing the stresses in the normal situation (Figure 26 to 30) to that in the multiple birth syndrome (Figure 37 to Figure 41) it can be seen that there is a general increase in the shear stresses especially shear stresses in the 1.3 plane. Also there is a very high tensile maximum and intermediate principal and shear stress at the first valley location near the location where the surface pressure was applied. Compressive stresses, seen at the inner surface of the sutures in the normal situation, are less than those seen in this case. It is interesting to note that high shear stresses are seen in the case of mastication in which tension is put on the cranium. This confirms the belief that mastication increases shear stress and put tensile stress on the sutures to result in increased fractal dimensions. This phenomenon can then also be said to be true for multiple birth syndrome.

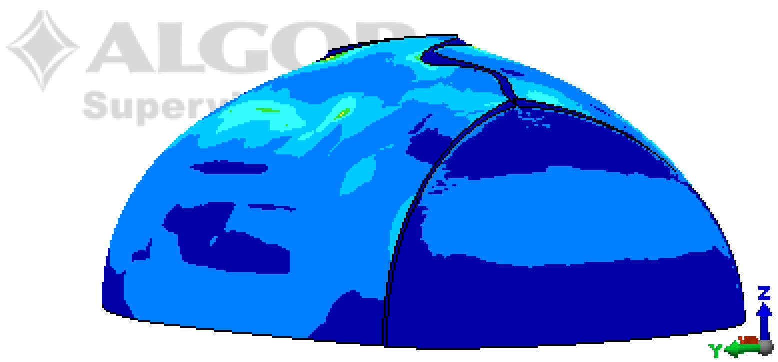

Figure 36 Contour plot of the stress distribution in the deformed model showing a dent in the side where surface pressure was applied.

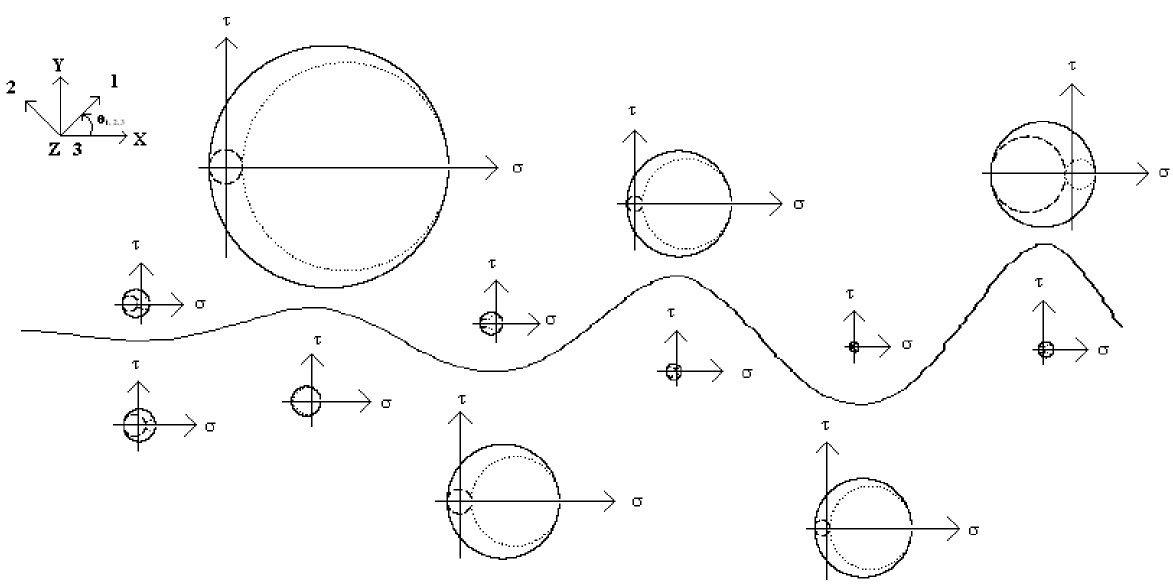

Figure 37 3D Mohr's circles of stresses (dotted circles = stresses on 1.3 plane, short dash circles = stresses on 1.2 plane, continuous circle = stresses on 2.3 plane.) at peak and valley locations along the sagittal suture on layer one. See appendix for orientations of principal stresses.

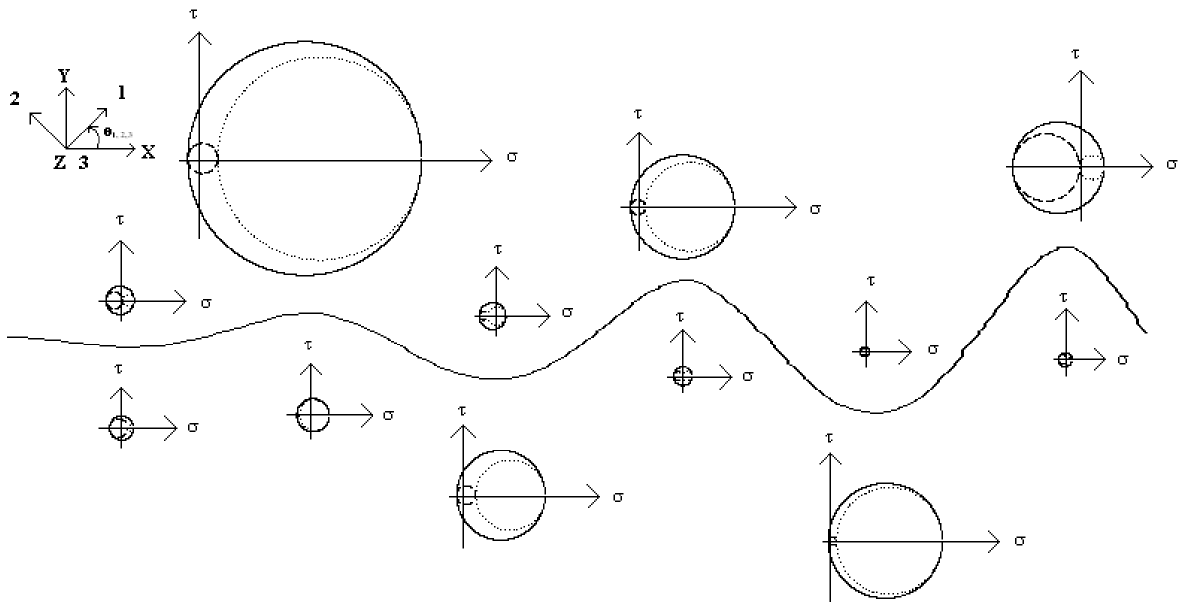

Figure 38 3D Mohr's circles of stresses (dotted circles = stresses on 1.3 plane, short dash circles = stresses on 1.2 plane, continuous circle = stresses on 2.3 plane.) at peak and valley locations along the sagittal suture on layer two. See appendix for orientations of principal stresses.

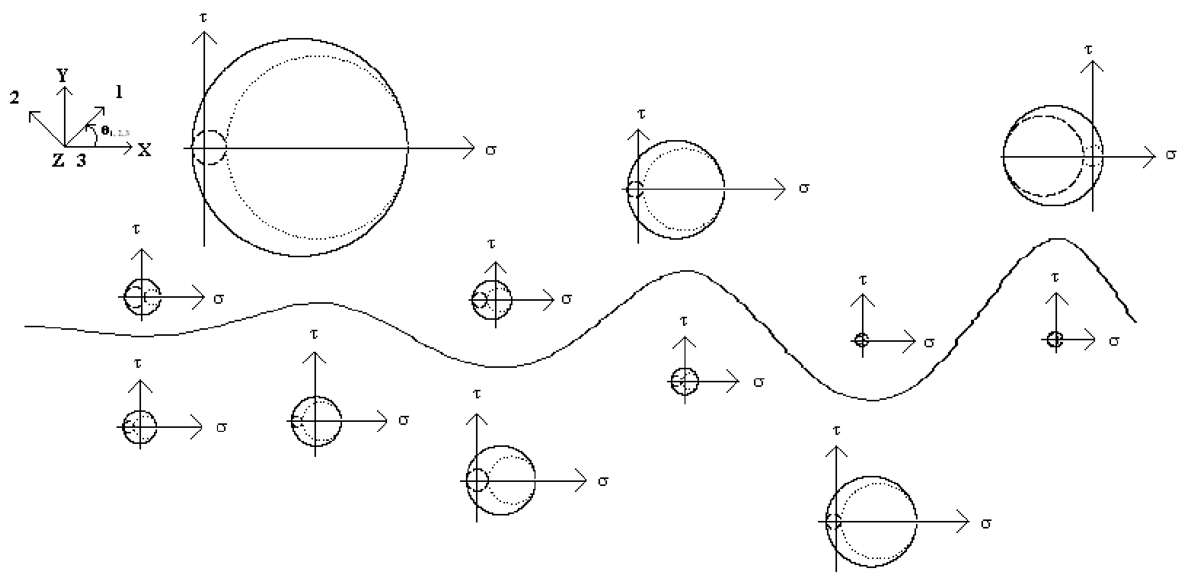

Figure 39 3D Mohr's circles of stresses (dotted circles = stresses on 1.3 plane, short dash circles = stresses on 1.2 plane, continuous circle = stresses on 2.3 plane.) at peak and valley locations along the sagittal suture on layer three. See appendix for orientations of principal stresses.

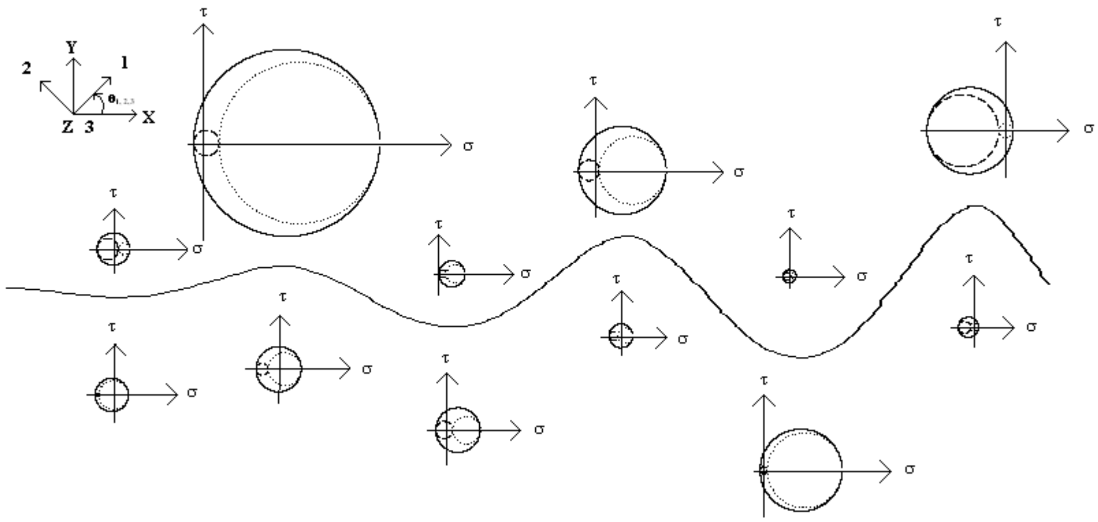

Figure 40 3D Mohr's circles of stresses (dotted circles = stresses on 1.3 plane, short dash circles = stresses on 1.2 plane, continuous circle = stresses on 2.3 plane.) at peak and valley locations along the sagittal suture on layer four. See appendix for orientations of principal stresses.

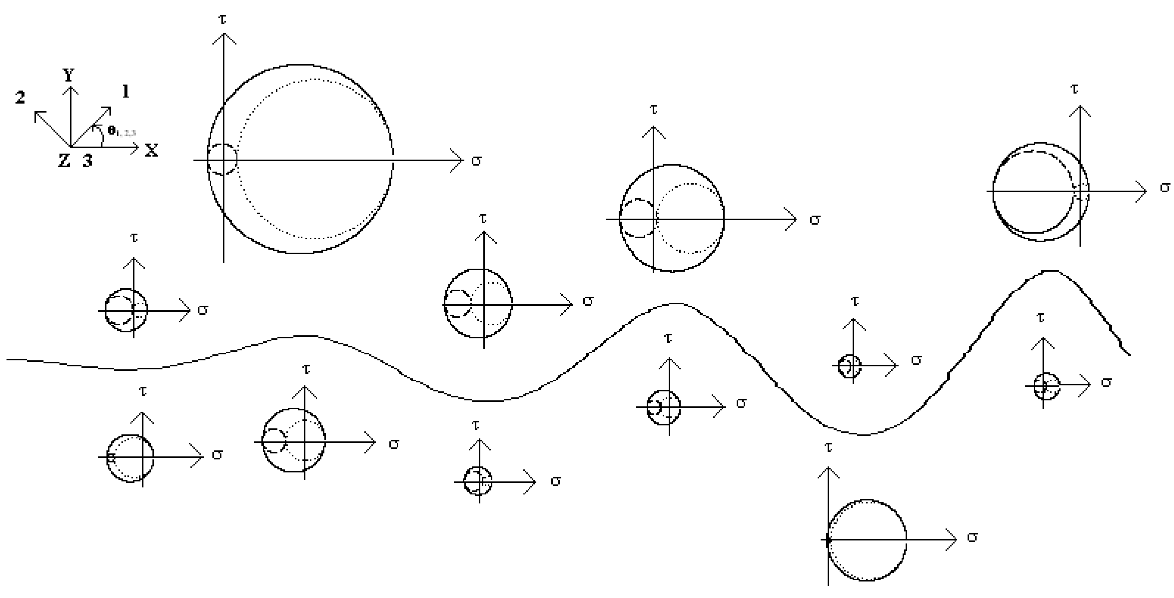

Figure 41 3D Mohr's circles of stresses (dotted circles = stresses on 1.3 plane, short dash circles = stresses on 1.2 plane, continuous circle = stresses on 2.3 plane.) at peak and valley locations along the sagittal suture on layer five. See appendix for orientations of principal stresses.

Table 1 Showing the expected stress levels in cranial models with one or more of the sutures fused and a cranium with patent sutures. Note the expected increase in the stresses when one or more sutures are fused. (A,B,C,D are stresses in the patent sutures and a,b,c,d are expected increases in A,B,C,D in the cranium when one or more of the sutures are fused)

VARIOUS SYNOSTOSIS	**PATENT SUTURES**	**CORONAL SYNOSTOSIS**	**LAMBDOID SYNOSTOSI**	**BICORONAL SYNOSTOSIS**	**SCAPHOCEPHALY**
	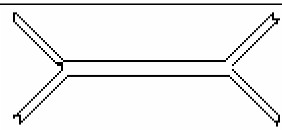	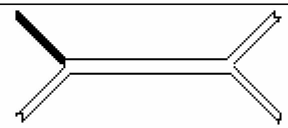	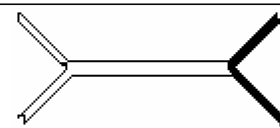	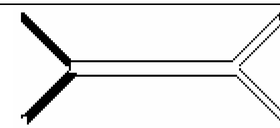	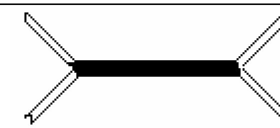
STATE DURING SYNOSTOSIS	ALL SUTURES PATENT (NO FUSION)	RIGHT CORONAL SUTURE (RCS) FUSED.	BOTH LAMBDOID SUTURES (LS) FUSED	BOTH CORONAL SUTURES (CS) FUSED	SAGITTAL SUTURE (SS) FUSED
STRESS LEVEL IN RIGHT CORONAL SUTURE	$\lvert A \rvert$		$\lvert A+a \rvert$		$\lvert A+a_1 \rvert$
STRESS IN LEFT CORONAL SUTURE	$\lvert B \rvert$	$\lvert B+b \rvert$	$\lvert B+b_1 \rvert$		$\lvert B+b_2 \rvert$
STRESS LEVEL IN SAGITTAL SUTURE	$\lvert C \rvert$	$\lvert C+c \rvert$	$\lvert C+c_1 \rvert$	$\lvert C+c_2 \rvert$	
STRESS LEVEL IN LAMBDOID SUTURES	$\lvert D \rvert$	$\lvert D+d \rvert$		$\lvert D+d_1 \rvert$	$\lvert D+d_2 \rvert$

Various forms of Synostosis

Brain growth coupled with other stress inducing factors increases the ICP in the cranium. A cranium with all the sutures patent will remodel to accommodate the growing brain and also to keep the ICP at physiologically safe levels. Remodeling occurs when the sutures sense the increase in pressure and induce bone formation to cause the cranial bone plates to grow resulting in a corresponding increase in the volume of the cranium. In the event of one or more of the sutures fusing, the remodeling of the cranium is inhibited resulting in a disproportionate growth of the cranium with respect to the growing brain. When this occurs there is increase in the ICP and the higher the number of fused sutures the higher the increase in ICP. When a suture fuses prematurely in a cranium the other patent sutures takes over the remodeling of the cranium. Cranial bones that are prematurely fused act as a single bone plate with decreased growth potential. Sutures adjacent to the fused suture compensate in growth more than sutures distant from it. Since ICP increases when one or more of the sutures fuse, there is expected to be an increase in the stress levels sensed by the patent sutures in a cranium with one or more sutures fused than they would normally sense when all the sutures are patent. To be able to capture the increase in stress levels, stresses along the bone/suture interface of a patent suture in a cranium with one or more suture fused is compared to the stress levels along that same suture in a cranium with all the sutures patent. For example in a cranium with the sagittal suture fused, the stress levels along the two coronal and two lambdoid sutures will be compared to the stress levels along the two coronal and two lambdoid sutures in a cranium with the sagittal suture patent. Again for a cranium with the two coronal sutures fused, the stress levels along the sagittal and the two lambdoid sutures will be compared to the stress levels along the sagittal and lambdoid sutures in a cranium with the two coronal sutures patent.

Table 1 shows an outline of how the increase in stress levels was determined. Column two in Table 1 shows a cranium with all the sutures patent and the corresponding stress levels (A, B, C, D); column three shows a cranium with coronal synostosis (right coronal suture fused) and the expected increase in the stress levels in the remaining patent sutures (B+b, C+c, D+d); column four shows a cranium with lambdoid synostosis (both lambdoid sutures fused) and the expected increase in the stress levels in the remaining patent sutures (A+a, B+b_1, C+c_1); column five shows a cranium with bicoronal synostosis (both coronal sutures fused) and the expected increase in the stress levels in the remaining patent sutures (C+c_2, D+d_1); column six shows a cranium with scaphocephaly (sagittal suture fused) and the expected increase in the stress levels in the remaining sutures (A+a_1, B+b_2, D+d_2). To ascertain an increase in the stress levels in bicoronal synostosis, the stress levels in the sagittal, and two lambdoid sutures in the cranium with bicoronal synostosis (column five) is compared to the stress levels in sagittal and lambdoid sutures in a cranium with all the sutures patent (column two). Therefore from the table the increase in the stress levels in the patent sagittal and lambdoid sutures in bicoronal synostosis will be c_2 and d_1 respectively. Curves of the stresses along the sagittal suture in the bicoronal synostosis and the sagittal suture in the cranium with all sutures patent is plotted on the same graph to determine which suture has the highest stress levels. Similarly two more plots are obtained for the two lambdoid sutures. As already known there are five layers on each bone/suture interface in the model of the cranium. Therefore stress levels are determined on three of the layers (layer1, layer3 and layer5). Also the deformed models of the sutures in a cranium with synostosis are compared to the deformed models of the same sutures in the cranium with patent sutures. This is done to ascertain which suture (the same suture in a cranium with synostosis and the same suture in a cranium with all sutures patent) has the most deformation.

Coronal synostosis

The deformed and undeformed models (Figure 42 and Figure 43) of the cranial sutures in the cranium with coronal synostosis were obtained. Comparing these two figures it is clear that there is deformation in all the sutures but the right coronal suture, which was fused. Comparing the deformed model of the sutures in a cranium with coronal synostosis (Figure 43) to the deformed model in the cranium where all the sutures were patent (Figure 44) it is difficult to tell which sutures have the largest deformation. Therefore to determine which sutures have the most deformation the stress values along the interface between the cranial bones and sutures in both cases were obtained from the model.

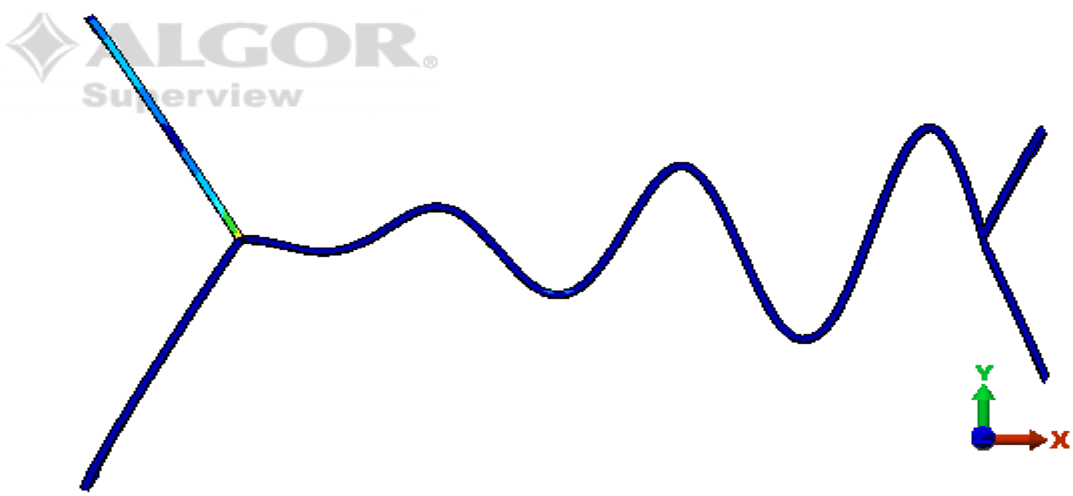

Figure 42 Contour plots of the stress distribution in the undeformed model of the cranial sutures showing the fused right coronal suture with higher stresses.

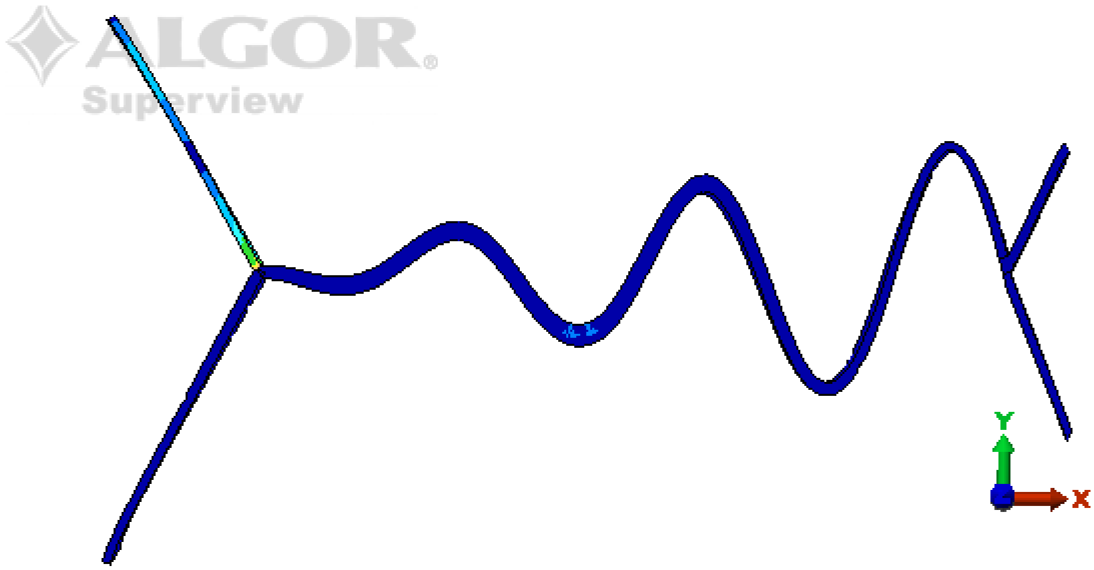

Figure 43 Contour plots of the stress distribution in the deformed model of the cranial sutures showing deformations in the sagittal and lambdoid sutures.

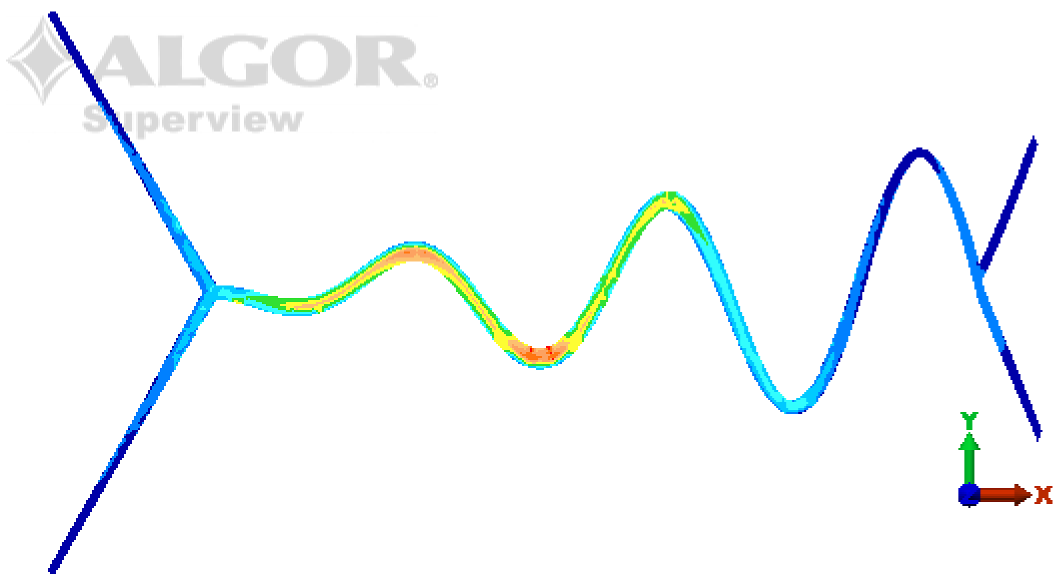

Figure 44 Contour plots of the stress distribution in the deformed model of patent cranial sutures.

Plots of the stress values along the sutures for both cases were then obtained (Figure 45 to Figure 48) to determine which model had the highest stress. Since stress is directly proportional to strain, increase in stress values can be said to be an increase in strain. In this case stress values along the interface of the left coronal suture and the frontal bone, along the interface of the right parietal bone and sagittal suture and along the interface of the left and right lambdoid sutures and the occipital bone were obtained. On some of the plots the values of the stresses on the different layers were too close and so values of 0.2 and 0.4 were added to the third and fifth layers respectively to distinguish them from one another. From the plots of the stresses on the interface of the frontal bone and the left coronal suture it is clear that (Figure 45) the stresses in the coronal synostosis case is higher on all layers than in the case where the sutures are patent. This shows that there is also more strain and deformation in the coronal suture in the coronal synostosis case. Observing the plots of the stresses on the interface of the right parietal bone and the sagittal suture in the two cases (Figure 46), it can be seen that the stresses in the sagittal suture in the coronal synostosis are higher in some locations and lower in other locations than the stresses in the sagittal suture in the cranium with all the sutures patent. It can therefore be said that the stresses in this plot is also higher. The plots at the interface of the left and right lambdoid sutures and the occipital bone for both cases (cranium with bicoronal synostosis and cranium with all sutures patent) shows that the stresses are almost the same at most locations and is just a little higher at other locations (Figure 47 and Figure 48). This is expected since these sutures are further away from the fused suture. Therefore the fusion of the right coronal suture led to the increase in the stresses on the interface of the other sutures and the adjacent bones.

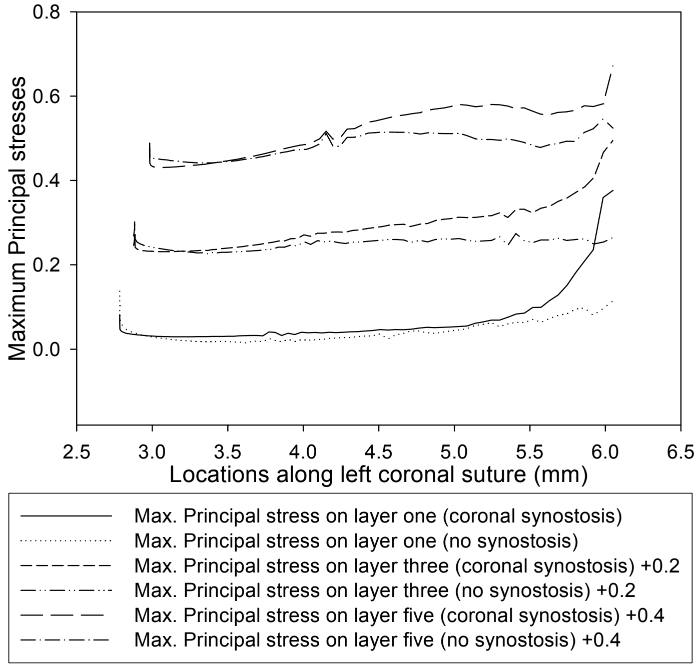

Figure 45 Plot of the maximum principal stress along the interface of the left coronal suture and the frontal bone for the model with coronal synostosis and the model with all the sutures patent.

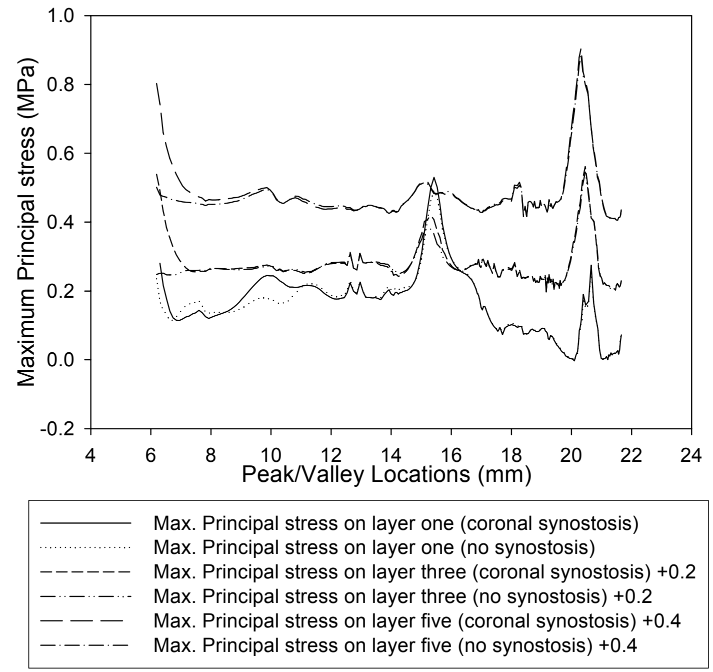

Figure 46 Plot of the maximum principal stress along the interface of the sagittal suture and the right parietal bone for the model with coronal synostosis and the model with all the sutures patent.

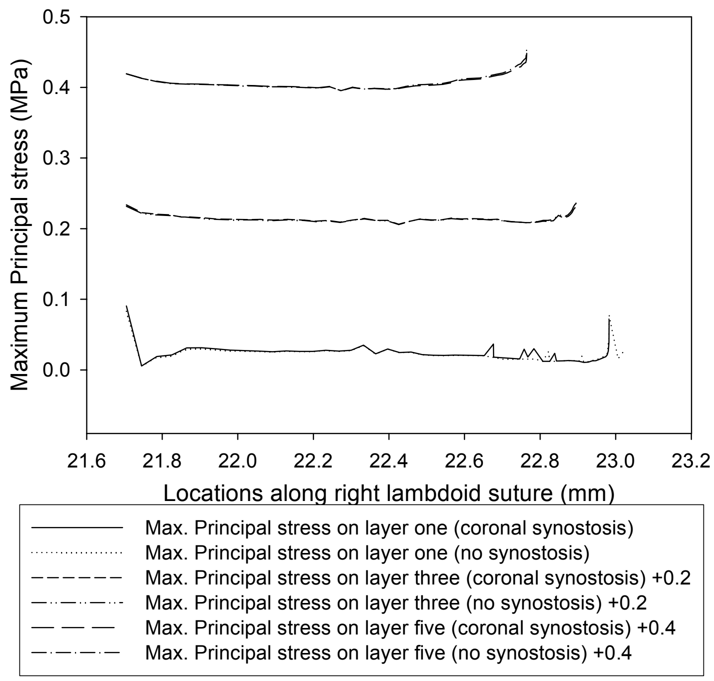

Figure 47 Plot of the maximum principal stress along the interface of the right lambdoid suture and the occipital bone for the model with coronal synostosis and the model with all the sutures patent.

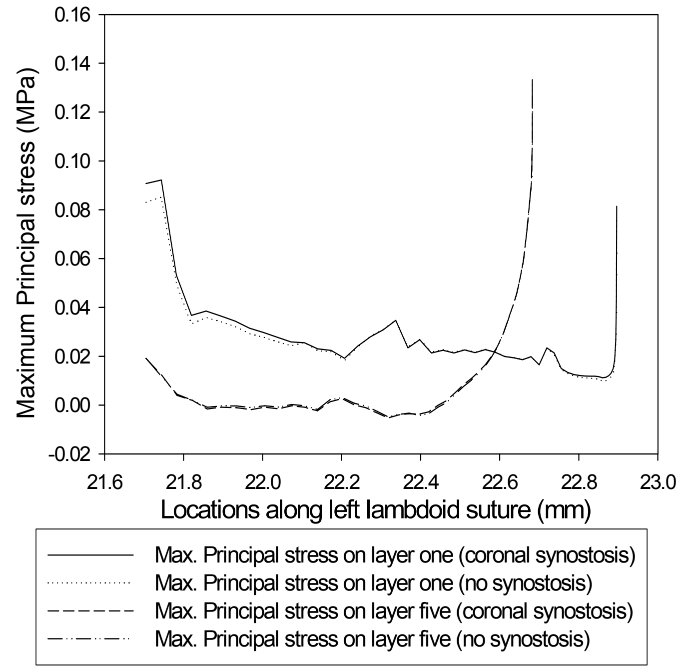

Figure 48 Plot of the maximum principal stress along the interface of the left lambdoid suture and the occipital bone for the model with coronal synostosis and the model with all the sutures patent.

Also the percentage increase in the stress levels in left coronal, sagittal and lambdoid sutures when the right coronal suture is fused was computed. The stress levels in the left coronal suture showed an increase of 42.86%. Those in the sagittal suture showed an increase of 4.31% and for the lambdoid sutures the stress levels went up by 2.4%. It is interesting to see a higher percentage increase in the suture (left coronal suture) nearest to the fused suture (right coronal suture) than those further away from it (sagittal and lambdoid sutures). Clinically, premature synostosis of one of the coronal sutures causes an asymmetric forehead and brow. On the side where the suture is fused the forehead is flattened and recessed and the other side undergoes compensatory bulging (Bronfin D.R, 2001; Martin H.S et al., 1997; Majid A.K et al., 2003; Raj D.S et al., 2001). From the above results apart from the left coronal suture there is not much raise in the stresses on the sagittal and lambdoid sutures. This implies that there will be more growth at the bone plates bothering the coronal suture than at those bothering the other sutures resulting in bulging of one side of the forehead. Therefore the results are consistent with what happens *in vivo.*

Lambdoid Synostosis

As it was done in the coronal synostosis, the deformed and undeformed models of the cranial sutures (Figure 49 and Figure 50) were compared to see the deformations in the sutures that were left patent. Also the deformed model of the cranial sutures in the model with lambdoid synostosis (Figure 50) was compared to the deformed model of the sutures in the cranial model with all the sutures patent (Figure 44). It was difficult to detect any difference, thus plots of the stresses on the bone/suture interface of the two coronal and sagittal sutures (for both the cranium with lambdoid synostosis and the cranium with all sutures patent) was used to detect the difference in stress values.

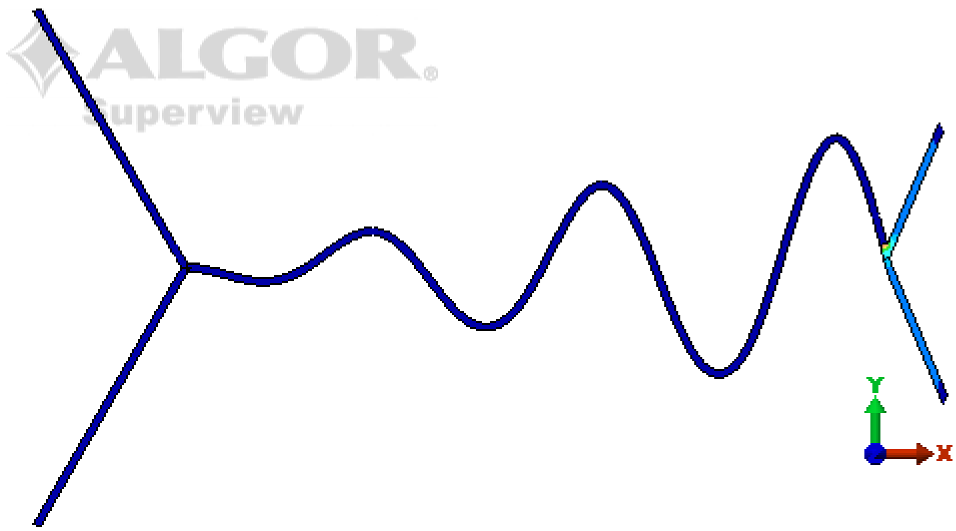

Figure 49 Contour plots of the stress distribution in the undeformed model of the cranial sutures showing the fused lambdoid sutures with higher stresses.

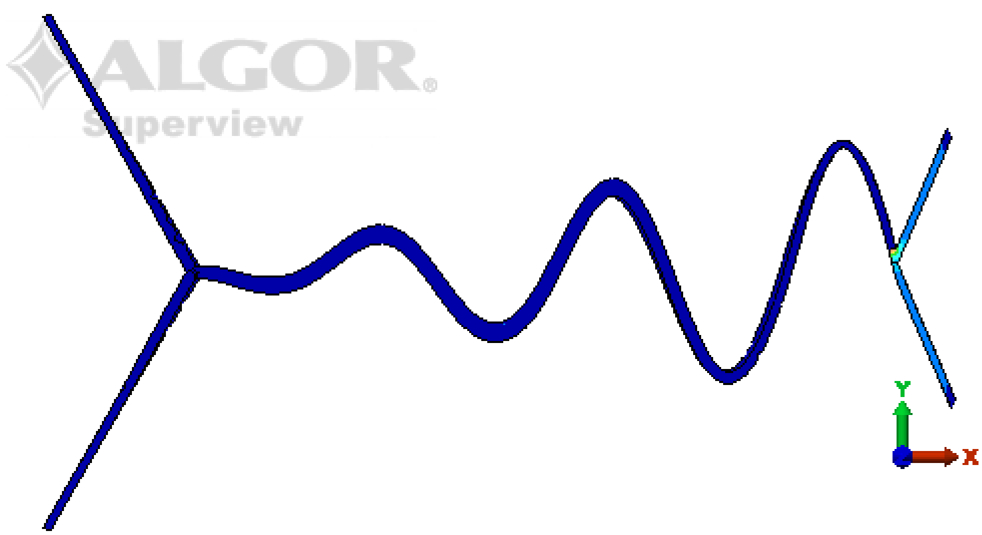

Figure 50 Contour plots of the stress distribution in the deformed model of the cranial sutures showing deformation in the coronal and sagittal sutures.

It can be seen that with the exception of the stresses on the fifth layer on the interface of the right coronal suture and frontal bone interface, the stresses on other layers are almost the same (Figure 52). The reverse is true for the stresses on the left coronal suture and frontal bone interface (Figure 53) where apart from the first layer the stresses on the other layers are the same. Looking at the plot of the stresses on the interface of the right parietal bone and the sagittal suture (Figure 51) for the model with fused lambdoid sutures and the model where all the sutures are patent, it can be seen that the stress levels are almost the same. Computing the percentage increase in the stress levels along the sagittal and coronal sutures in lambdoid synostosis, the stress levels in the sagittal suture increased by 2.69%, those in the right coronal suture by 11.39% and those in the left coronal suture went up by 13.15%. So the effect of fusion of the lambdoid sutures is felt more on the coronal sutures than on the sagittal suture. Clinically, lambdoid synostosis results in a trapezoid look of the head when viewed from above and also the posterior end of the skull is flattened. There is also increased vertical growth to accommodate brain development (Bronfin D.R, 2001; Martin H.S et al., 1997; Majid A.K et al., 2003; Raj D.S et al., 2001). Correlating the physiological outcome of this synostosis to the results, it can be said that the observed higher stresses in the coronal suture will result in higher growth rates of the frontal bones and adjacent sides of the parietal bones. This type of growth, coupled with growth at the sagittal suture and flattening of the posterior end due to the fusion of the lambdoid sutures, will result in the trapezoid look of the head. This result is therefore consistent with what actually happens *in vivo*.

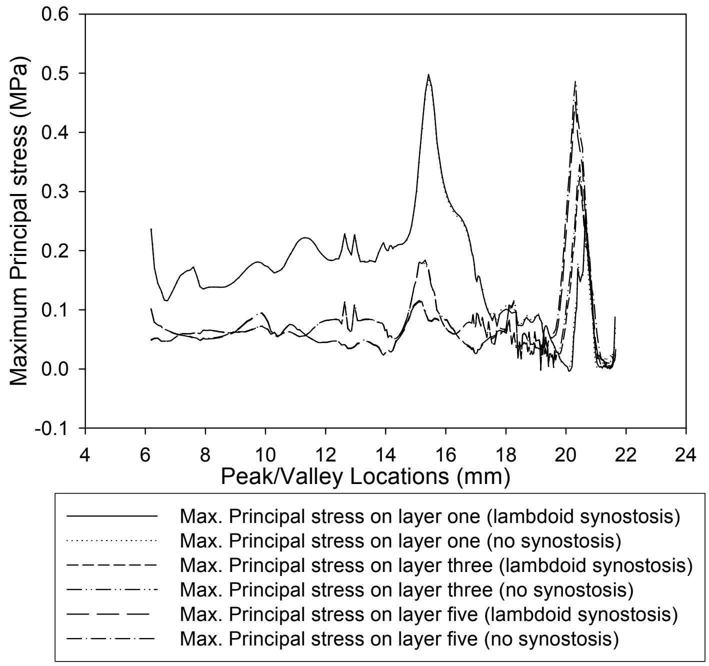

Figure 51 Plot of the maximum principal stress along the interface of the sagittal suture and the right parietal bone for the model with lambdoid synostosis and the model with all sutures patent.

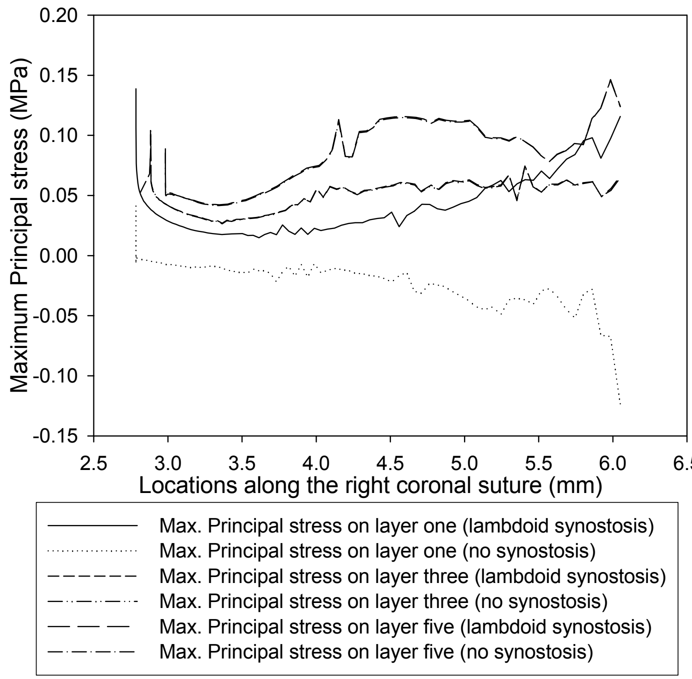

Figure 52 Plot of the maximum principal stress along the interface of the right coronal suture and the frontal bone for the model with lambdoid synostosis and the model with all the sutures patent.

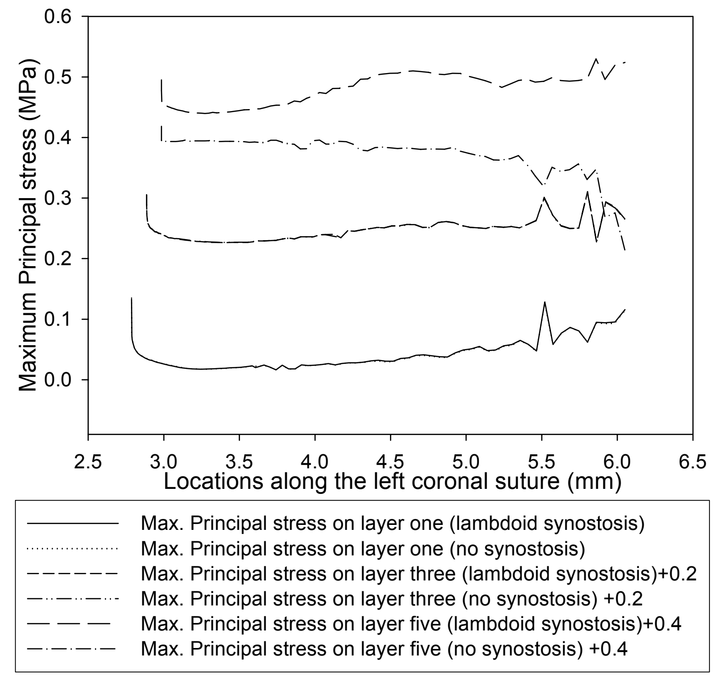

Figure 53 Plot of the maximum principal stress along the interface of the left coronal suture and the frontal bone for the model with lambdoid synostosis and the model with all the sutures patent.

Bicoronal synostosis

Comparing the deformed and undeformed models of the cranial sutures (Figure 54 and Figure 55), it can be seen that there is deformation in all the sutures but the two coronal sutures. Comparing the deformed model of the cranial sutures in the cranium with bicoronal synostosis (Figure 55) to the deformed model of the sutures in the cranium where all the sutures are patent (Figure 44), it is difficult to observe a significant increase in deformation. So stress values were obtained at the cranial bone/suture interfaces for the sagittal and lambdoid sutures for both models (cranium with bicoronal synostosis and cranium with all sutures patent) to help detect the increase in stress levels. From these stresses, plots were obtained to determine which model had the higher stress values (Figure 56). From the plot it can be seen that in most locations the stresses are higher than the stresses in the model where all the sutures were patent. Computing the percentage increase in the stress levels in the sagittal and lambdoid sutures gave an increase of 0.76% in the stress levels of the sagittal suture and 0.23% increase in the stress levels of the lambdoid sutures. This indicates that the sagittal suture will compensate in growth more than the lambdoid sutures. Clinically, this kind of synostosis results in a flat retruded forehead, increased height to the skull and increased biparietal diameter (Bronfin D.R, 2001; Martin H.S et al., 1997; Majid A.K et al., 2003; Raj D.S et al., 2001). The flat retruded forehead is due to the fusion of the coronal sutures. And also the increased height to the skull and increased biparietal diameter can be linked to the increase in stress levels seen in the sagittal suture in the model of the cranium with bicoronal synostosis. Since the increase in stress levels is observed in the locations of the cranium where compensatory growth occurs during bicoronal synostosis, the results obtained can be said to be consistent with what happens *in vivo*.

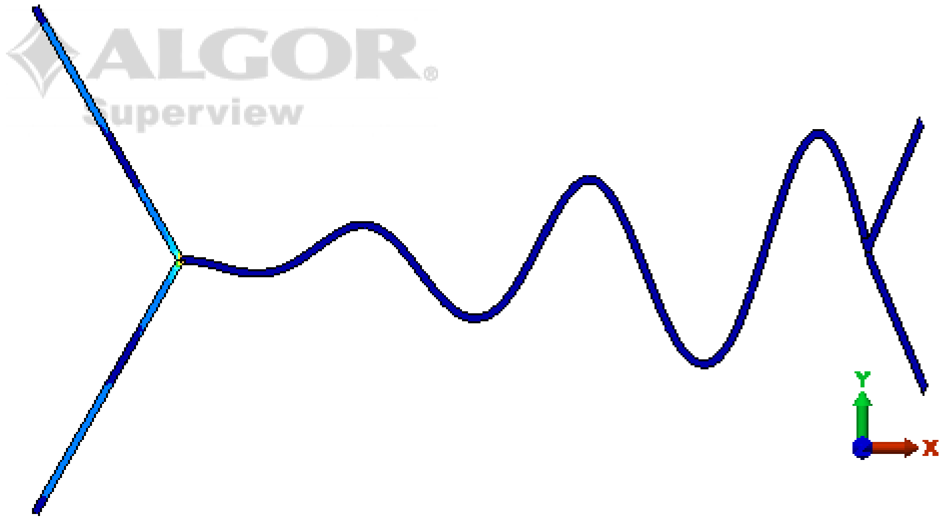

Figure 54 Contour plots of the stress distribution in the undeformed model of the cranial sutures showing the fused coronal sutures with higher stresses.

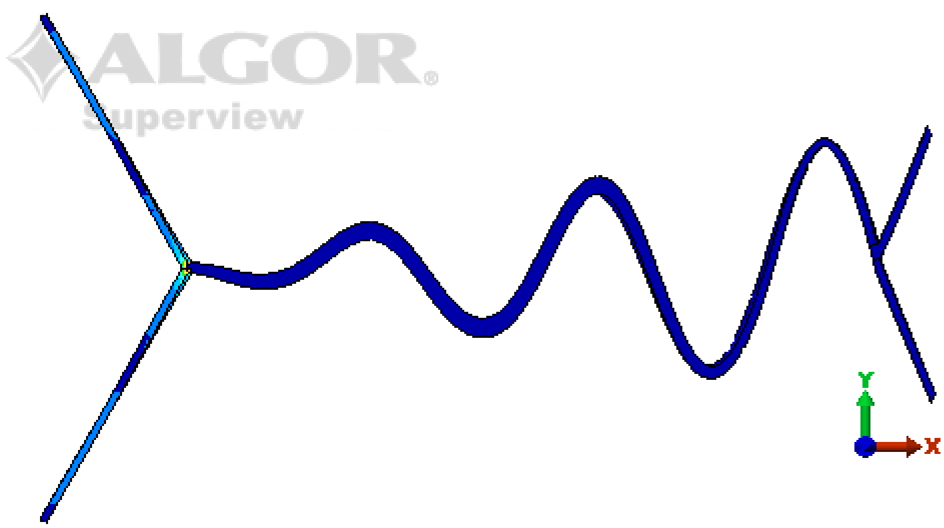

Figure 55 Contour plots of the stress distribution in the deformed model of the cranial sutures showing deformations in the sagittal and lambdoid sutures.

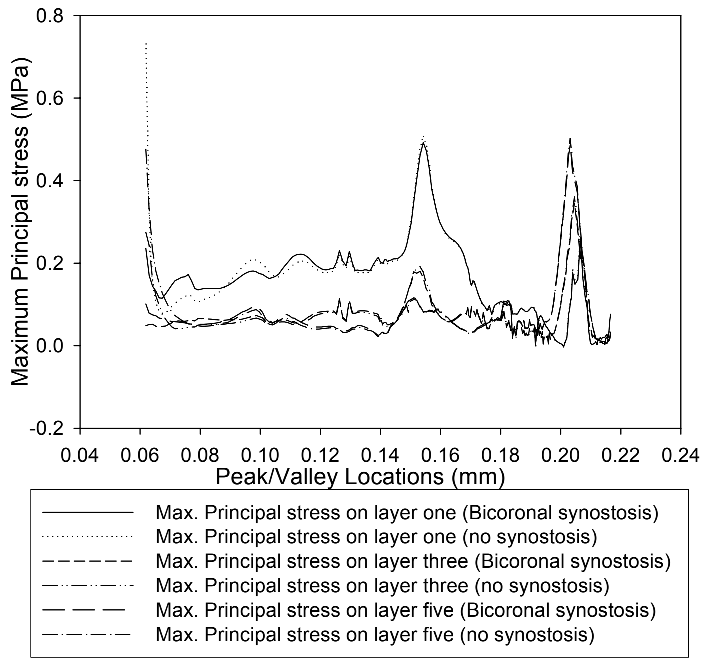

Figure 56 Plot of the maximum principal stress along the interface of the sagittal suture and the right parietal bone for the model with bicoronal synostosis and the model with all the sutures patent.

Scaphocephaly

Again comparing the deformed and undeformed models (Figure 57 and Figure 58) it could be seen that there is deformation in all the sutures but the sagittal suture which was fused. Being unable to tell from visual observation by comparing the deformed model of cranial sutures in the cranium with scaphocephaly to that of the model of the cranium with patent sutures (Figure 44), the distribution of the stresses in the two cases are plotted together to determine which of the cases have the higher stress values. From the plots (Figure 59 and Figure 60) it can be said that the stress distribution in simulated scaphocephaly case are higher than those with sutures patent. From Figure 61 and Figure 62 it can be seen that stresses on all the layers are mostly higher. The percentage increase in the stress levels of the coronal sutures in scaphocephaly was found to be 19.03% and that of the lambdoid sutures was 14.83%.

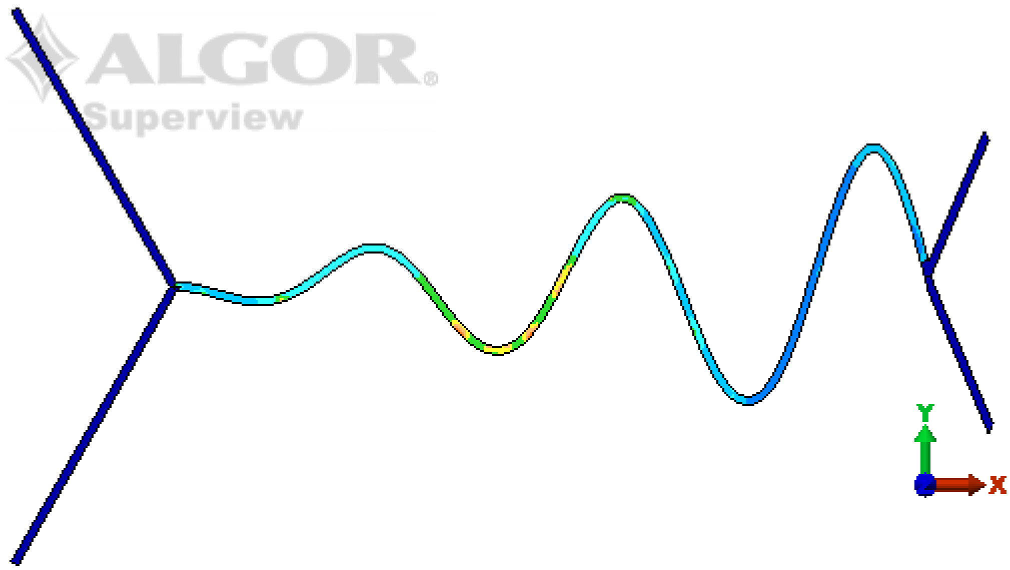

Figure 57 Contour plots of the stress distribution in the undeformed model of the cranial sutures showing the fused sagittal suture with higher stresses.

Clinically, when scaphocephaly occurs lateral growth stops and this results in a narrow head. However, compensatory growth occurs in the anteroposterior direction. This compensatory growth causes a bulging in the front and the back of the head that results in elongation of the skull (Bronfin D.R, 2001; Martin H.S et al., 1997; Majid A.K et al., 2003; Raj D.S et al., 2001). The compensatory growth can be attributed to the increase in the stresses in the patent coronal and lambdoid sutures which results in growth of all the bone plates in contact with them thus producing a narrow head. Therefore the increase in the stress levels in the coronal and lambdoid sutures is consistent with what happens *in vivo*.

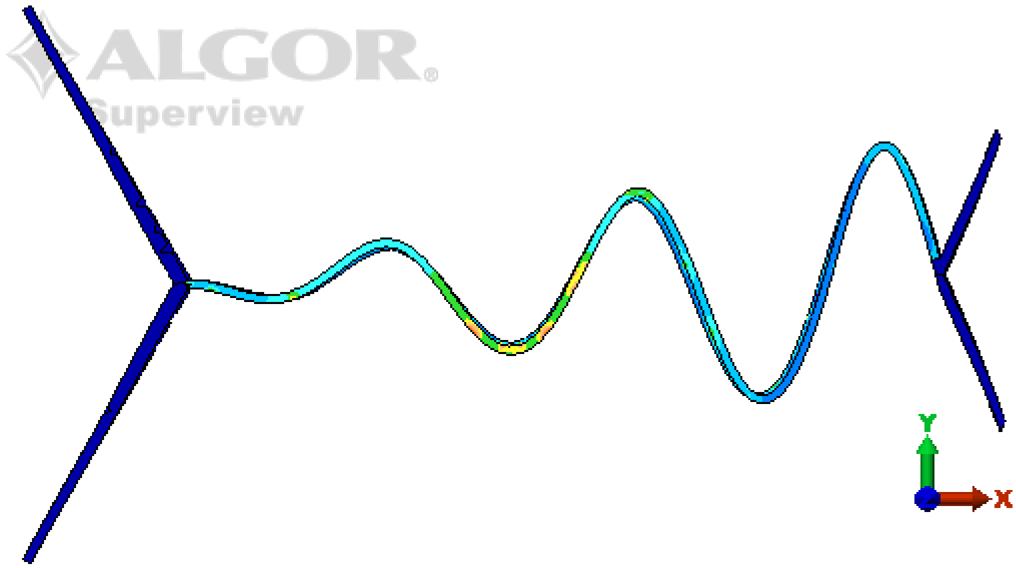

Figure 58 Contour plots of the stress distribution in the deformed model of the cranial sutures showing deformations in the two coronal and lambdoid sutures.

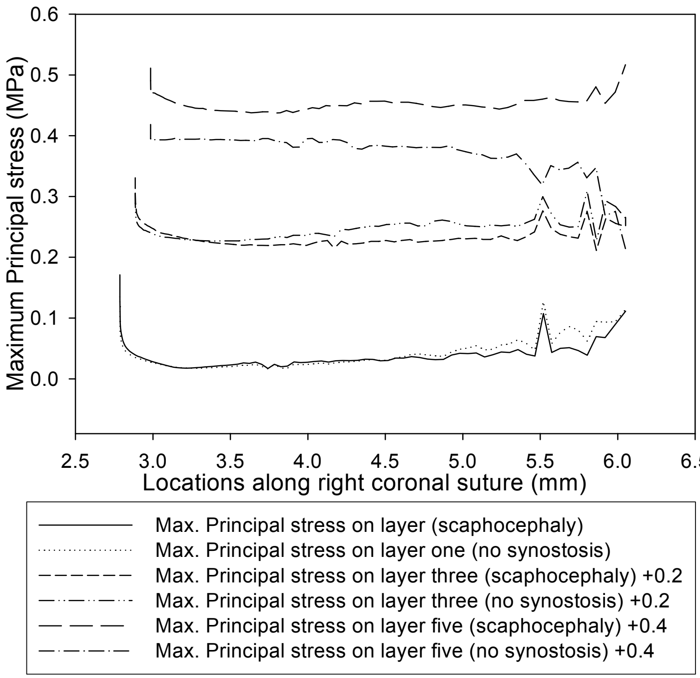

Figure 59 Plot of the maximum principal stress along the interface of the right coronal suture and the frontal bone for the model with scaphocephaly and the model with all the sutures patent.

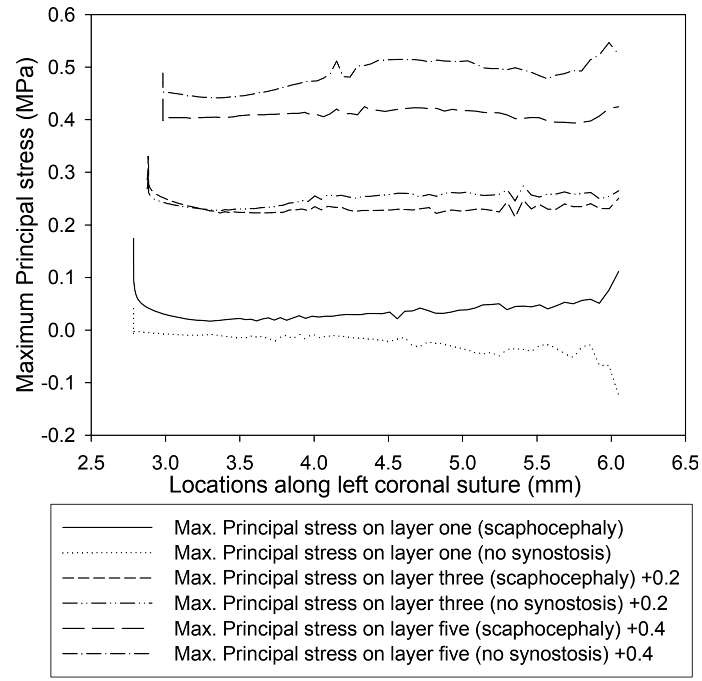

Figure 60 Plot of the maximum principal stress along the interface of the left coronal suture and the frontal bone for the model with scaphocephaly and the model with all the sutures patent.
.

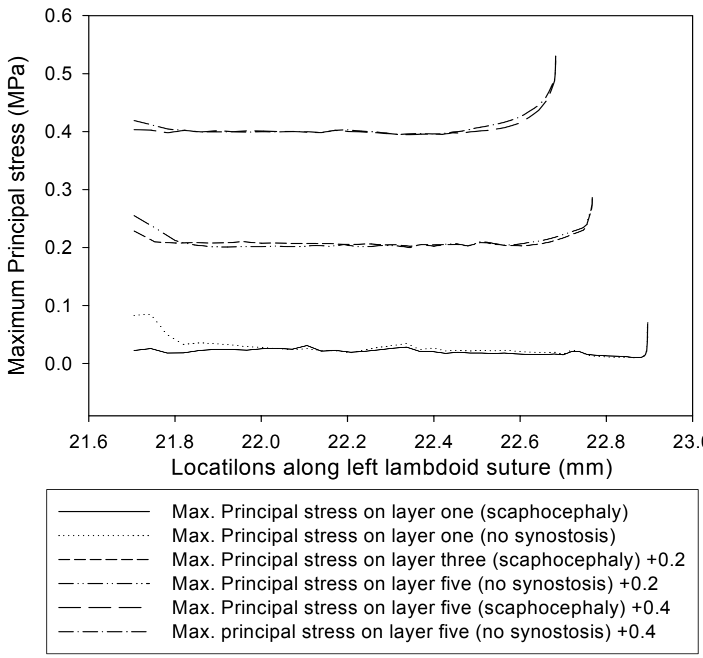

Figure 61 Plot of the maximum principal stress along the interface of the left lambdoid suture and the occipital bone for the model with scaphocephaly and the model with all the sutures patent.

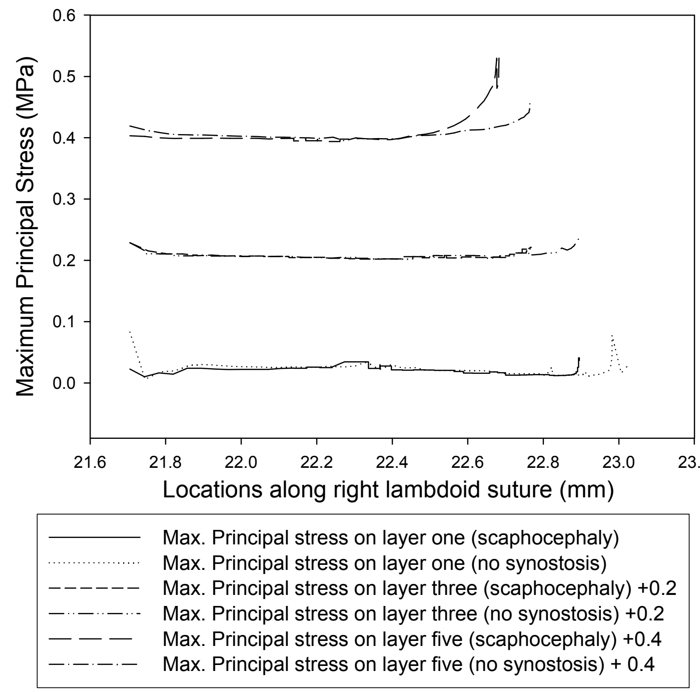

Figure 62 Plot of the maximum principal stress along the interface of the right lambdoid suture and the occipital bone for the model with scaphocephaly and the model with all the sutures patent.

CHAPTER 7

CONCLUSIONS

The purpose of this research was to investigate the stress states at the bone/suture interface in the cranium. Thus 2D and 3D models of the cranium were built and various analyses were performed on them. The stress states at the interface of the cranial bones and sutures were then determined using Mohr's circles. Also a possible link between the morphology of the sutures and the internal stress states was discussed.

From the 2D study, high shear stresses cause bone resorption and normal stresses cause bone formation. Also as the amplitude of the wavy suture pattern increases the shear stress increases causing more bone resorption and the normal stress drops. This suggests that the formation of suture interdigitation and the further increase in its complexity may be to relieve the principal tension in order for the cranial bone fronts to reach new equilibrium and minimum stress states.

Adding the interphase to the model did not alter the stress distribution pattern and the location of the Mohr's circles. However there is a relatively higher tensile stress along the interface. It can therefore be said that adding an interphase to the model did not have a significant impact on the stress distribution along the interface.

It can be said from the simulation of fusion that fusion of sutures causes the stresses on the interface (which is usually higher than the applied load depending on the complexity of the interdigitation) to drop to a value closer to the externally applied load. Thus the fusion of sutures may be to relieve extensive stresses exerted on it. The stresses on either sides of the suture also tend to approach a common value. Interestingly as the suture fuses the normal stress on the side of the suture where bone resorption might be, changes from biaxial tensile compressive to biaxial tensile stresses. Those on the side which may be undergoing bone formation also stay biaxial tensile. As the stress components and their magnitudes become the same there is neither bone formation nor resorption and at that stage there is complete fusion.

The highest stress obtained in the nonlinear analysis was 4.5KPa, which is much less than the yield stress of bone of about 50MPa. The load used in this analysis was 3.33KPa. Also to show the nonlinearity of bone material a load of 24MPa was used. This yielded a curve that fell out of the elastic region of the stress strain curve for bone (Figure19),thus showing the nonlinear nature of bone. However this pressure if it existed in the cranium exceeds the blood pressure and thus blood will cease to flow to the brain and this will result in death. This suggests that even though bone is a nonlinear material, under normal physiological loading in the cranium nonlinearity will not occur.

The stress distribution along the bone/suture interface in the 3D model of the cranium indicates that there is a high tensile stress in the upper surface of the suture, and a high compressive stress in the inner surface. This nature of stress distribution in the 3D model sheds light on the reasons why the pattern of interdigitation on the outer surface of the sutures are different from that on the inside, and also explains why suture fusion starts from the inside surface of a cranium sutures. Furthermore, the morphology of the suture pattern is not governed by only stress components on one plane but a combination of the stress components on all the three planes of action. Also the first peak locations of the wavy suture pattern showed higher shear stresses than the opposite side (receding valley). This should not be the case since high shear stresses results in bone resorption therefore the side with higher shear is expected to show bone resorption but not formation. Interestingly the side with a higher shear stress also has a higher normal stress. It can thus be speculated that there is a threshold of shear or normal stress above which bone resorption or formation will occur regardless of the magnitude of normal or shear stress respectively.

Also, the stress distribution along the bone/suture in the case of infants is not much different from that in the adult. It should however be said that some of the material properties used for the infant case were assumed. This assumption was made due to the unavailability of material properties for human infant bone and suture properties.

It has been observed that in the case of chewing that high shear stresses exist on the sagittal suture/bone interface. These high shear stresses are due to the tensile stress generated at the interface due to the pulling of the muscles attached to the bone plates during mastication. In the case of multiple birth pregnancies, where sometimes the heads are together, high tensile stresses are generated at the bone/suture interface with increase in shear stresses. These high stresses, as observed in the 3D Mohr's circles for the multiple birth syndrome, explains why synostosis occurs in most multiple birth pregnancies.

From the plots and deformed models of the sutures in the simulation of the various synostosis, it is clear that there is a general increase in the stress values of the sutures in the neighborhood of the fused sutures. This buttresses the belief that when a suture fuses, the patent sutures close to it remodel to help dissipate some of the high stresses generated as a result of the fusion.

The above conclusions suggest that the stress states at the bone/suture interface govern the mechano-morphogenesis of the cranial bones and sutures. Knowledge of these stresses will help determine the nature of the stress states and maginitudes that results in the known biochemical processes which result in craniosynostosis. This will help in decoding the cause and to better treat craniosynostosis.

CHAPTER 8

FUTURE DIRECTIONS

The pattern of the sagittal suture used in the 3D model was the same one used in the 2D study, which is not proportional to the dimensions of the cranium. This was used to enable a comparison between the 2D and 3D studies. Therefore a future study will be conducted with a sagittal suture pattern that is proportional to the cranium. Also in this study cyclic loading will be considered.

Based on the fore knowledge of the stress components and level corresponding to bone formation and resorption, a future study should take an approach to simulate mechano-morphogenesis in cranial development. This can be done in such a way that whenever the element senses a certain stress component (could be a combination of different stress components) above or below a particular magnitude it will undergo bone formation or bone resorption. The advantage of such a study is that one would be able to see the cranium grow and also track the mechano-morphogenesis of the cranial sutures.

Experimental measurements of the local stress states at the cranial bone/suture interface are necessary for validating the models. This can be achieved by exploiting the micro/nano fabrication techniques to develop micro/nano scale mechanical sensors for localized, high-precision and simultaneous multi-variable measurements. These sensors could then be used to measure the mechanical environments at the bone/suture interface in vivo in normal physiological loading conditions.

This will present the capability to perform actual experiments to determine the component and magnitude of stress that is required to keep a suture patent and the nature and magnitude of stress that causes it to synostose.

REFERENCES

1. Abe, H, Hayashi, K, Sato, M. 1996. Data Book on Mechanical Properties of Living Cells, Tissues, and Organs. Springer-Verlag Tokyo.
2. Alderman, B.W, Lammer E.J, Joshua,S.C. 1998. An epidemiologic study of craniosynostosis: Risk indicators for the occurrence of craniosynostosis in Colorado. Am. J. Epidemiol. 128: 431.
3. Aliberti, F.P, Ruggiero, L. Cinalli, C. Maggi, G. 2002. The treatment of the positional plagiocephaly with a new thermoplastic orthotic device. Childs Nervous System. 18(6-7): 337-9.
4. Argenta, L.C.K, David, L.R, Wilson, J.A, Bell, W.O. 1996. An increase in infant cranial deformity with supine sleeping position. J. Craniofacial. Surgery. 7: 5.
5. Aviv R.I, Rodger E, Hall C.I, 2001. Craniosynostosis.
6. Bass, J.K, Bass, W.T, Green, G.A, Gurtner, P, White, L.E. 2003. Intracranial Pressure Changes During Intermitten CSF Drainage. Pediatric Neurology; 173-177.
7. Baxter, L, Moran, T.H, Richtsmeier, J.T, Troncoso, J, Reeves, R.H. 2000. Discovery and genetic localization of Down syndrome cerebellar phenotypes using the Ts65Dn mouse. Human Molecular Genetics 9(2): 195-202.
8. Bayraktar, H.H, Morgan, E.F, Niebar, G.L, Morris, G.E, Wong, E.K, Keaveny, T.M, 2003. Comparison of the elastic and yield properties of human femoral trabecullar and cortical bone

9. Borke, J.L, Yu, J.C, Orellana, M.F. 2000. Mechanotransductin: a possible role for plasmamembrane disruption. Boston: Harvard Society for the Advancement of Orthodontics. 43-48.
10. Bronfin, D.R. 2001. Misshappen Heads in Babies: Position or Pathology? The Ochsner Journal; 3:191-199.
11. Burrows, A.M, Richtsmeier, J.T. Mooney, M.P, Smith, T.D, Losken, H.W. Siegel, M.I. 1999. Three-Dimensional Analysis of Craniofacial Form in a Familial Rabbit Model of Nonsyndromic Coronal Suture Synostosis Using Euclidean Distance Matrix Analysis. Craniofacial Journal. 36; 3: 196-206.
12. Chalmers, J. and Ray, R.D.,1962. The growth of transplanted foetal bones in different immunological environments, J. Bone Joint Surgery, 44B, 149-164.
13. Chen, H. 2002. Crouzon Syndrome.
14. Chen, J, Zhong, Q, Wang, J, Cameron, R.S, Borke, J. L, Isales, C.M, Bollag, R.J. 2001. Microarray Analysis of Tbx2-directed Gene Expression: a Possible Role in Osteogenesis. Ireland: Elsvier Science: 43-54.
15. Cohen, M.. J. 2001. Asymmetry: molecular, biologic, embryopathic, and clinical perspectives. American Journal of Medical Genetics. 101(4): 292-314.
16. Cowin S.C. 2001. Bone Mechanics Handbook. CRC Press
17. Craig, R.R. 2000. Mechanics of Materials, 2nd ed. New York : John Wiley & Sons.
18. Currey J.1984. The Mechanical Adaptation of Bones. Princeton University Press.
19. Ellenbogen, R.G, Cunningham, M.L. 2000. Update on craniofacial surgery: the differential diagnosis of lambdoid synostosis/posterior plagiocephaly. Clincal Neurosurgery. 47: 303-18.

20. Enlow, D.H. 2000. Normal craniofacial growth. In Cohen MMJ, MacLean RE, editors. Craniosynostosis: diagnosis, evaluation, and management, 2nd ed. NewYork:Oxford University Press. 35-50.

21. Enlow, D.H.1975. Handbook of facial growth. Philadelphia, W.B. Saunders.

22. Fell, H.B, 1956. Skeletal development in tissue culture, in the Biochemistry and Physiology of Bone, Academic Press, New York.

23. Frost, H.M. 1963. Bone remodeling dynamics.

24. Gilbert, J.L, Kennel, J, Zhang, G, Stern, P.H. 1999. Strain Dependent Non-Linear Viscoelastic Micromechanics and Biological Response of Viable Week-old Mouse Tibia, Transactions of the Society For Biomaterial, p532.

25. Hamrock,B.J, Schmid, S.R, Jacobson, B. 1999. Fundamentals of Machine Elements, 2nd ed. New York: McGraw-Hill.

26. Henderson, J.H, Carter, D.R. 2002. Mechanical Induction in Limb Morphogenesis: The Role of Growth-Generated Strains and Pressures. Bone; Vol. 31, No.6:645-653.

27. Henderson, J.H, Longaker, M.T, Carter, D.R. 2003. Sutural Bone Deposition Rate and Strain Magnitude During Cranial Development. Elsvier, Inc. 1-10.

28. Herring, S.W, Rafferty, K.L, Liu, Z.J, Marshall, C.D. 2001. Jaw Muscles and the Skull in Mammals: the Biomechanics of Mastication. Comparative Biochemistry and Physyiology Part A1313; 207-219.

29. Huang, M.H.S, Mouradian, W.E, Cohen, S.R, Gruss, J.S. 1998. Craniofacial Journal; 35: 204-211.

30. Hyer, M. 1998. Stress Analysis of Fiber-Reinforced Composite Materials, McGraw-Hill.

31. Jans, G, Audekercke,R.V, Sloten, J.V, Gobin, R, Van der Perre, G, Mommaerts, .Y. Bending Properties of Cranial Bone Segments of New-born Children.
32. Kelly, K.L, T.R. Pomatto, J.K. Manwaring, K.H. Beals, S.P. 1999. Cranial growth unrestricted during treatment of deformational plagiocephaly. Pediatric Neurosurgery. 30(4): 193-9.
33. Khan, A.M, Weltman, D.I, Webber, B.J, Balsam, D. 2003. Craniosynostosis.
34. Klein-Nulend, J, Veldhuijzen, J.P, de Jong, M, Burger, E.H. 1987. Inreased bone formation and decreased bone resorption in fetal mouse calvaria as a result of intermittent compressive force in vitro. Bone Miner. 2: 441.
35. Martin, R.B, Burr, D.B, Sharkey, N.A. 1997. Skeletal Tissue Mechanics. New York: Springer-Verlag.
36. Martínez-Lage, J.F, Alamo, L, Poza, M. 1999. Raised intrarcranial pressure in minimal forms of craniosynostosis. Child's Nervous System; 15:11-16.
37. Martínez-Lage, J.F, Poza, M, Lluch, T. 1996. Craniosynostosis in Neural Tube Defects: A Theory on its Pathogenesis. New York: Elsevier Science Inc. 465-470.
38. Miller, R.C, S.K. 2000. Long-term developmental outcomes in patients with deformational plagiocephaly. Pediatrics. 105(2): E26.
39. Opperman, L.A. 2000. Cranial sutures as intramembranous bone growth sites. Developmental. Dynamics 219(4): 472-85.
40. Pashley, D.H, Borke, J.L, Yu, J. 2002. Biomechanics and Craniofacial Morphogensis. Craniofacial Sugery; 6:84-95.

41. Perlyn, C.M, J.L. Vannier, M.W. Kane, A.A. Koppel, P. Clark, K.W. 2001. The craniofacial anomalies archive at St. Louis Children's Hospital: 20 years of craniofacial imaging experience. Plastic & Reconstructive Surgery. 108(7): 1862-70.
42. Porter, D. 2004. Pragmatic multiscale modeling of bone as a natural hybrid nanocomposite. Materials Science & Engineering A365; 38-45.
43. Richtsmeier, J.T, Zumalt, A, Carlson, E.J, Epstein, C.J, Reeves, R.H. 2002. Craniofacial Phenotypes in Segmentally Triosomic Mouse Models for Down Syndrome. American Journal of Medical Genetics; 107: 317-324.
44. Richtsmeier, J.T, Zumwalt, A, Carlson, E.J, Epstein, C.J, Reeves, R.H. 2002. Craniofacial phenotypes in segmentally trisomic mouse models for Down syndrome. Am.J.Med.Genet. 107(4): 317-24.
45. Richtzmier, J.T, Grausz, H. M, Morris, G.R, Marsh, J.L, Vannier, M.W. 1991. Growth of the Cranial Base in Craniosynostosis. 28; 1:55-67.
46. Rooker, S, Jorens, P.G, Reempts, J.V, Borgers, M, Verlooy, J. 2003. Continuous Measurement of Intracranial Pressure in Awake Rates After experimental Closed Head Injury. Journal of Neuroscience Methods; 131: 75-81.
47. Sgouros, S. 2003. Craniosynostosis.
48. Shahinian, H.K, Jaekle, R, Suh, R.H, Jarrahy, R, Aguilar, V.C, Soojian, M. Skull Base Institute; 1-18
49. Shapiro, D, Richtsmeier, J.T. 1997. Brief Communication: A Sample of Pediatric Skulls Available for Study. American journal of physical anthropology. 103: 415-417.
50. Sheth, D.R, Iskandar, J.B, 2001. Craniosynostosis.

51. Shieh, J, Chou, C, Huang, S, Kao, M. 2003. Intracranial Pressure Model in Intensive Care Unit Using a Simple Recurrent Neural Network Through Time.

52. Smalt, R, Mitchell, F.T, Howard, R.L, Chambers, T.J. 1997. Induction of NO and Prostaglandin E2 in Osteoblasts by Wall-shear Stress but not Mechanical Strain. 751-758.

53. Turk, A.E, McCarthy, J.G, Thorne, C.H.M, Wisoff, J.H. 1996. The “Back to sleep caMPaign” and deformational plagiocephaly: Is there case for concern? J. Craniofac.Surg. 7:12.

54. Vu, H.P, J. Parker, E.E. Levine, N.S. Franel, P. 2001. The timing of physiologic closure of the metopic suture: a review of 159 patients using reconstructed 3D CT scans of the craniofacial region. Journal of Craniofacial Surgery. 12(6): 527-32.

55. Williams J.K, Ellenbogen R.G, Gruss J.S,1999. State of the Art in Craniofacial Surgery: Non-syndromic Craniosynostosis

56. Williams, J.K, Ellenbogen, R.G, Gruss, J.S. 1999. State of the Art in Craniofacial Surgery: Nonsyndromic Craniosynostosis. 484-485.

57. Wolfe, A. 2000. Congenital Synostoses.

58. Yu, J.C, Braselton, J, Abel, M, Borke, J.L. The Identification of Calcium Oscillators in Immature Rat Cranial Sutures.

59. Zhang, G, Latour, R.A Jr.1994.An Analytical and Numerical Analysis of Fiber Microbuckling. Composite Science and Technology, Vol.51, p95-109.

60. Zhang, G, Stern, P.H, Lautenschlager, E.P, Gilbert, J.L. 1996. In-vitro Micromechanical Behavior of Viable Neonatal Mouse Tibia. Trans. the fifth World Biomaterials Congress, p392.

61. Zumpano, M.P, Benjamin, S.C, Marsh, J.L, Vanderkolk, C.A, Richtsmeier, J.T. 1999. Three-Deimensional Morphological Analysis of Isolated Metopic Synostosis. The Anatomical Record; 256:177-188.

APPENDIX

Orientations of the Maximum Principal Stresses on the 3D Mohr's circles for the model of the Adult Cranium

Table 2 Showing the orientations (θ_1, orientations on plane 2.3, θ_2, orientations on plane 1.3, θ_3 orientations on plane 1.2) of the maximum principal stresses along the upper and lower interfaces of the wavy suture pattern for layer one.

LOCATIONS ALONG SUTURE PATTERN			1	2	3	4	5	6
UPPER INTERFACE	Continuous circles	θ_1	8.46	-22.86	36.46	-17.00	28.86	-19.26
	Dotted circles	θ_2	13.14	5.65	-12.99	-13.06	45.00	45.00
	Short dashed circles	θ_3	37.80	-8.42	12.18	11.60	-0.85	7.28
LOWER INTERFACE	Continuous circles	θ_1	4.47	-25.84	12.36	-27.06	3.91	-32.51
	Dotted circles	θ_2	14.04	4.36	-5.42	9.97	45.00	-21.61
	Short Dashed circles	θ_3	45.00	4.33	-33.40	-0.08	45.00	-7.54

Table 3 Showing the orientations (θ_1, orientations on plane 2.3, θ_2, orientations on plane 1.3, θ_3, orientations on plane 1.2) of the maximum principal stresses along the upper and lower interfaces of the wavy suture pattern for layer two.

LOCATIONS ALONG SUTURE PATTERN			1	2	3	4	5	6
UPPER INTERFACE	Continuous circles	θ_1	24.15	-24.14	27.91	-34.44	31.83	-19.52
	Dotted circles	θ_2	45.00	7.34	-13.92	-21.09	-12.67	45.00
	Short dashed circles	θ_3	13.71	-0.26	-3.92	18.65	-30.41	7.52
LOWER INTERFACE	Continuous circles	θ_1	18.03	-29.38	14.48	-23.90	16.79	-33.36
	Dotted circles	θ_2	45.00	3.34	-9.22	-1.64	45.00	-6.86
	Short Dashed circles	θ_3	-15.13	-3.90	-37.74	-12.04	7.50	-16.45

Table 4 Showing the orientations (θ_1, orientations on plane 2.3, θ_2, orientations on plane 1.3, θ_3, orientations on plane 1.2) of the maximum principal stresses along the upper and lower interfaces of the wavy suture pattern for layer three.

LOCATIONS ALONG SUTURE PATTERN			1	2	3	4	5	6
UPPER INTERFACE	Continuous circles	θ_1	45.00	-32.41	35.58	-17.22	31.67	-14.86
	Dotted circles	θ_2	45.00	30.91	-20.57	45.00	-9.74	45.00
	Short dashed circles	θ_3	8.28	9.75	18.96	11.60	-24.25	8.93
LOWER INTERFACE	Continuous circles	θ_1	16.33	-30.63	35.95	-27.58	26.74	-27.82
	Dotted circles	θ_2	45.00	-4.05	-8.63	-22.61	45.00	-25.84
	Short Dashed circles	θ_3	6.46	-4.44	2.87	7.15	-6.58	-24.57

Table 5 Showing the orientations (θ_1, orientations on plane 2.3, θ_2, orientations on plane 1.3, θ_3, orientations on plane 1.2) of the maximum principal stresses along the upper and lower interfaces of the wavy suture pattern for layer four.

LOCATIONS ALONG SUTURE PATTERN			1	2	3	4	5	6
UPPER INTERFACE	Continuous circles	θ_1	1.88	-18.49	38.49	-16.81	21.52	-12.07
	Dotted circles	θ_2	17.47	26.31	-6.08	45.00	-5.09	-40.87
	Short dashed circles	θ_3	-2.48	-0.37	-15.50	4.49	45.00	-7.04
LOWER INTERFACE	Continuous circles	θ_1	14.96	-39.56	15.95	-28.26	28.55	-0.89
	Dotted circles	θ_2	31.31	4.43	-11.20	0.45	45.00	45.00
	Short Dashed circles	θ_3	26.47	-1.77	17.54	-1.39	-13.02	-17.78

Table 6 Showing the orientations (θ_1, orientations on plane 2.3, θ_2, orientations on plane 1.3, θ_3 orientations on plane 1.2) of the maximum principal stresses along the upper and lower interfaces of the wavy suture pattern for layer five.

LOCATIONS ALONG SUTURE PATTERN			1	2	3	4	5	6
UPPER INTERFACE	Continuous circles	θ_1	-3.39	-16.71	25.59	-17.82	32.12	-33.52
	Dotted circles	θ_2	45.00	21.93	-21.75	-45.00	-17.49	45.00
	Short dashed circles	θ_3	-35.82	24.62	19.77	9.29	45.00	-1.97
LOWER INTERFACE	Continuous circles	θ_1	18.95	-32.98	7.43	-14.86	33.85	-28.24
	Dotted circles	θ_2	22.50	18.82	-8.05	19.76	45.00	45.00
	Short Dashed circles	θ_3	27.98	-29.39	9.68	45.00	-26.25	-10.17

Orientations of the Maximum Principal Stresses on the 3D Mohrs circles for the model of the Infant Cranium

Table 7 Showing the orientations (θ_1, orientations on plane 2.3, θ_2, orientations on plane 1.3, θ_3, orientations on plane 1.2) of the maximum principal stresses along the upper and lower interfaces of the wavy suture pattern for layer one.

LOCATIONS ALONG SUTURE PATTERN			1	2	3	4	5	6
UPPER INTERFACE	Continuous circles	θ_1	1.94	-0.50	3.54	-0.61	8.88	-1.49
	Dotted circles	θ_2	11.63	7.06	-1.01	-9.44	-6.26	-45.00
	Short dashed circles	θ_3	12.65	1.97	0.85	-22.25	4.64	4.09
LOWER INTERFACE	Continuous circles	θ_1	-1.34	-2.22	0.35	-4.09	-2.38	-16.85
	Dotted circles	θ_2	21.50	1.04	-0.55	-2.53	-25.00	-10.47
	Short Dashed circles	θ_3	-17.35	1.43	-1.41	0.41	44.89	-38.89

Table 8 Showing the orientations (θ_1, orientations on plane 2.3, θ_2, orientations on plane 1.3, θ_3, orientations on plane 1.2) of the maximum principal stresses along the upper and lower interfaces of the wavy suture pattern for layer two.

LOCATIONS ALONG SUTURE PATTERN			1	2	3	4	5	6
UPPER INTERFACE	Continuous circles	θ_1	5.32	-3.59	8.59	-2.86	11.69	-6.00
	Dotted circles	θ_2	20.05	45.00	-2.62	-19.58	1.12	-45.00
	Short dashed circles	θ_3	1.99	0.94	0.99	-0.11	-0.20	-17.58
LOWER INTERFACE	Continuous circles	θ_1	-0.90	-6.99	3.09	-9.67	1.17	-13.78
	Dotted circles	θ_2	45.00	1.25	-1.09	-1.95	-45.00	-7.53
	Short Dashed circles	θ_3	-5.84	0.81	-0.67	-0.25	17.41	-20.94

Table 9 Showing the orientations (θ_1, orientations on plane 2.3, θ_2, orientations on plane 1.3, θ_3, orientations on plane 1.2) of the maximum principal stresses along the upper and lower interfaces of the wavy suture pattern for layer three.

LOCATIONS ALONG SUTURE PATTERN			1	2	3	4	5	6
UPPER INTERFACE	Continuous circles	θ_1	2.26	-8.19	9.74	-8.09	8.44	-5.91
	Dotted circles	θ_2	45.00	11.60	-5.69	45.00	2.83	-45.00
	Short dashed circles	θ_3	0.07	4.49	1.40	1.85	-3.21	-7.50
LOWER INTERFACE	Continuous circles	θ_1	2.97	-7.79	11.49	-9.40	2.65	-1.83
	Dotted circles	θ_2	45.00	1.61	-1.89	-3.13	45.00	-9.18
	Short Dashed circles	θ_3	0.73	0.67	3.40	-0.16	-0.45	-22.50

Table 10 Showing the orientations (θ_1, orientations on plane 2.3, θ_2, orientations on plane 1.3, θ_3, orientations on plane 1.2) of the maximum principal stresses along the upper and lower interfaces of the wavy suture pattern for layer four.

LOCATIONS ALONG SUTURE PATTERN			1	2	3	4	5	6
UPPER INTERFACE	Continuous circles	θ_1	-3.32	-5.58	5.04	-0.88	2.03	-4.06
	Dotted circles	θ_2	45.00	6.43	-20.79	45.00	-5.05	-45.00
	Short dashed circles	θ_3	-4.53	2.76	1.82	7.08	-7.11	-13.49
LOWER INTERFACE	Continuous circles	θ_1	4.87	-2.50	6.05	-3.44	0.36	-15.06
	Dotted circles	θ_2	31.54	8.69	-1.02	-4.48	-45.00	-37.93
	Short Dashed circles	θ_3	10.71	-0.47	6.59	1.26	-45.00	-17.06

Table 11 Showing the orientations (θ_1,orientations on plane 2.3, θ_2, orientations on plane 1.3, θ_3 orientations on plane 1.2) of the maximum principal stresses along the upper and lower interfaces of the wavy suture pattern for layer five.

LOCATIONS ALONG SUTURE PATTERN			1	2	3	4	5	6
UPPER INTERFACE	Continuous circles	θ_1	-3.32	-1.85	-2.04	-3.23	2.01	-8.39
	Dotted circles	θ_2	6.25	1.73	0.17	-10.08	-4.48	-45.00
	Short dashed circles	θ_3	-10.23	0.95	29.45	20.50	-23.36	-1.96
LOWER INTERFACE	Continuous circles	θ_1	2.57	2.31	2.13	4.81	5.25	-11.28
	Dotted circles	θ_2	12.47	3.00	-1.11	-9.88	-27.17	45.00
	Short Dashed circles	θ_3	45.00	-3.03	3.38	6.50	-45.00	-9.84

Orientations of the Maximum Principal Stresses on the 3D Mohrs circles for the model of the Multiple Birth Pregnancy

Table 12 Showing the orientations (θ_1 ,orientations on plane 2.3, θ_2, orientations on plane 1.3, θ_3 ,orientations on plane 1.2) of the maximum principal stresses along the upper and lower interfaces of the wavy suture pattern for layer one.

LOCATIONS ALONG SUTURE PATTERN			1	2	3	4	5	6
UPPER INTERFACE	Continuous circles	θ_1	9.22	-0.94	23.35	-2.47	45.00	-1.84
	Dotted circles	θ_2	12.65	0.84	-5.39	-10.59	-45.00	45.00
	Short dashed circles	θ_3	20.91	-7.14	-13.53	5.32	45.00	5.73
LOWER INTERFACE	Continuous circles	θ_1	17.91	-9.61	2.03	-45.00	0.20	-7.36
	Dotted circles	θ_2	20.91	-0.29	-0.23	-9.11	-14.95	-0.51
	Short Dashed circles	θ_3	-17.86	45.00	-7.49	2.61	45.00	3.33

Table 13 Showing the orientations (θ_1, orientations on plane 2.3, θ_2, orientations on plane 1.3, θ_3 ,orientations on plane 1.2) of the maximum principal stresses along the upper and lower interfaces of the wavy suture pattern for layer two.

LOCATIONS ALONG SUTURE PATTERN			1	2	3	4	5	6
UPPER INTERFACE	Continuous circles	θ_1	9.04	-1.73	45.00	-5.30	45.00	-1.32
	Dotted circles	θ_2	20.59	1.12	-4.01	-13.90	-22.11	45.00
	Short dashed circles	θ_3	-4.88	-4.82	-4.47	19.50	-0.14	-0.41
LOWER INTERFACE	Continuous circles	θ_1	5.49	-17.33	6.38	45.00	1.99	-10.98
	Dotted circles	θ_2	45.00	0.83	0.13	-8.40	-15.53	0.34
	Short Dashed circles	θ_3	-9.41	7.17	3.27	5.82	45.00	-3.52

Table 14 Showing the orientations (θ_1, orientations on plane 2.3, θ_2, orientations on plane 1.3, θ_3 orientations on plane 1.2) of the maximum principal stresses along the upper and lower interfaces of the wavy suture pattern for layer three.

LOCATIONS ALONG SUTURE PATTERN			1	2	3	4	5	6
UPPER INTERFACE	Continuous circles	θ_1	4.29	-2.90	-2.90	-2.90	19.88	-3.18
	Dotted circles	θ_2	20.16	1.48	-2.74	-18.17	-16.28	45.00
	Short dashed circles	θ_3	2.86	0.83	-1.40	10.71	-2.46	-0.92
LOWER INTERFACE	Continuous circles	θ_1	8.09	-14.56	13.81	-45.00	4.33	-8.17
	Dotted circles	θ_2	20.24	1.58	0.86	-8.12	-31.22	-1.57
	Short Dashed circles	θ_3	-2.95	3.42	5.28	7.62	-5.23	-5.43

Table 15 Showing the orientations (θ_1, orientations on plane 2.3, θ_2, orientations on plane 1.3, θ_3, orientations on plane 1.2)of the maximum principal stresses along the upper and lower interfaces of the wavy suture pattern for layer four.

LOCATIONS ALONG SUTURE PATTERN			1	2	3	4	5	6
UPPER INTERFACE	Continuous circles	θ_1	4.44	-3.16	45.00	-9.05	17.24	-3.45
	Dotted circles	θ_2	18.69	1.25	-3.50	-16.40	-19.86	45.00
	Short dashed circles	θ_3	-1.85	6.14	3.32	6.09	-11.68	-2.02
LOWER INTERFACE	Continuous circles	θ_1	6.49	-8.25	14.84	-22.09	6.04	-5.76
	Dotted circles	θ_2	10.21	0.91	0.41	-5.35	-34.35	-1.77
	Short Dashed circles	θ_3	34.44	-0.15	22.18	24.21	45.00	-5.17

Table 16 Showing the orientations (θ_1, orientations on plane 2.3, θ_2, orientations on plane 1.3, θ_3 orientations on plane 1.2) of the maximum principal stresses along the upper and lower interfaces of the wavy suture pattern for layer five.

LOCATIONS ALONG SUTURE PATTERN			1	2	3	4	5	6
UPPER INTERFACE	Continuous circles	θ_1	0.50	-1.60	4.25	-3.93	5.84	-4.88
	Dotted circles	θ_2	10.50	1.13	-1.44	-13.31	-14.58	45.00
	Short dashed circles	θ_3	-4.73	8.47	1.67	7.32	-18.69	-1.96
LOWER INTERFACE	Continuous circles	θ_1	2.66	-3.02	14.06	-6.19	9.24	-4.43
	Dotted circles	θ_2	5.50	0.85	-3.66	-1.62	-45.00	-0.26
	Short Dashed circles	θ_3	45.00	-2.08	37.12	12.48	-25.36	-7.27